JOURNAL OF QUATERNARY SCIENCE (2021) 1–28 ISSN 0267-8179. DOI: 10.1002/jqs.3295

JQS Journal of Quaternary Science QRA Quaternary Research Association

Timing and pace of ice-sheet withdrawal across the marine–terrestrial transition west of Ireland during the last glaciation

COLM Ó COFAIGH,[1]* S. LOUISE CALLARD,[1,2] DAVID H. ROBERTS,[1] RICHARD C. CHIVERRELL,[3] C. K. BALLANTYNE,[4] DAVID J. A. EVANS,[1] MARGOT SAHER,[5] KATRIEN J. J. VAN LANDEGHEM,[5] RACHEL SMEDLEY,[3] SARA BENETTI,[6] MATTHEW BURKE,[3] CHRIS D. CLARK,[7] GEOFF A. T. DULLER,[8] DEREK FABEL,[9] STEPHEN J. LIVINGSTONE,[7] STEPHEN MCCARRON,[10] ALICIA MEDIALDEA,[7] STEVEN G. MORETON[11] and FABIO SACCHETTI[12]

[1]Department of Geography, Durham University, Durham, UK
[2]Department of Geography, University of Newcastle, Newcastle, UK
[3]Department of Geography, University of Liverpool, Liverpool, UK
[4]School of Geography and Sustainable Development, University of St. Andrews, Scotland, UK
[5]School of Ocean Sciences, Bangor University, Menai Bridge, Wales, UK
[6]School of Geography and Environmental Sciences, Ulster University, Coleraine, Northern Ireland, UK
[7]Department of Geography, University of Sheffield, Sheffield, UK
[8]Department of Geography and Earth Sciences, University of Aberystwyth, Wales, UK
[9]Scottish Universities Environmental Research Centre, East Kilbride, Scotland, UK
[10]Department of Geography, Maynooth University, Co. Kildare, Ireland
[11]Natural Environment Research Council, Radiocarbon Facility, East Kilbride, Scotland, UK
[12]Marine Institute, Oranmore, Co. Galway, Ireland

Revised 4 February 2021; Accepted 12 February 2021

ABSTRACT: Understanding the pace and drivers of marine-based ice-sheet retreat relies upon the integration of numerical ice-sheet models with observations from contemporary polar ice sheets and well-constrained palaeoglaciological reconstructions. This paper provides a reconstruction of the retreat of the last British–Irish Ice Sheet (BIIS) from the Atlantic shelf west of Ireland during and following the Last Glacial Maximum (LGM). It uses marine-geophysical data and sediment cores dated by radiocarbon, combined with terrestrial cosmogenic nuclide and optically stimulated luminescence dating of onshore ice-marginal landforms, to reconstruct the timing and rate of ice-sheet retreat from the continental shelf and across the adjoining coastline of Ireland, thus including the switch from a marine- to a terrestrially-based ice-sheet margin. Seafloor bathymetric data in the form of moraines and grounding-zone wedges on the continental shelf record an extensive ice sheet west of Ireland during the LGM which advanced to the outer shelf. This interpretation is supported by the presence of dated subglacial tills and overridden glacimarine sediments from across the Porcupine Bank, a westwards extension of the Irish continental shelf. The ice sheet was grounded on the outer shelf at ~26.8 ka cal BP with initial retreat underway by 25.9 ka cal BP. Retreat was not a continuous process but was punctuated by marginal oscillations until ~24.3 ka cal BP. The ice sheet thereafter retreated to the mid-shelf where it formed a large grounding-zone complex at ~23.7 ka cal BP. This retreat occurred in a glacimarine environment. The Aran Islands on the inner continental shelf were ice-free by ~19.5 ka BP and the ice sheet had become largely terrestrially based by 17.3 ka BP. This suggests that the Aran Islands acted to stabilize and slow overall ice-sheet retreat once the BIIS margin had reached the inner shelf. Our results constrain the timing of initial retreat of the BIIS from the outer shelf west of Ireland to the period of minimum global eustatic sea level. Initial retreat was driven, at least in part, by glacio-isostatically induced, high relative sea level. Net rates of ice-sheet retreat across the shelf were slow (62–19 m a^{-1}) and reduced (8 m a^{-1}) as the ice sheet vacated the inner shelf and moved onshore. A picture therefore emerges of an extensive BIIS on the Atlantic shelf west of Ireland, in which early, oscillatory retreat was followed by slow episodic retreat which decelerated further as the ice margin became terrestrially based. More broadly, this demonstrates the importance of localized controls, in particular bed topography, on modulating the retreat of marine-based sectors of ice sheets. © 2021 The Authors. *Journal of Quaternary Science* Published by John Wiley & Sons Ltd.

KEYWORDS: British–Irish Ice Sheet; glacimarine sediments; ice sheet extent; ice sheet retreat; Last Glacial Maximum; Porcupine Bank; radiocarbon dating; subglacial till; western Ireland

Introduction

At its maximum around 27 ka BP during the last glacial period, the British–Irish Ice Sheet (BIIS) covered Ireland and much of Britain and had an ice volume with a sea level equivalent of ~2.5 m (Clark *et al.*, 2012). The ice sheet was drained by several large ice streams and extended onto the adjoining continental shelf including the North Sea where it coalesced with the Fennoscandian Ice Sheet

*Correspondence: Colm Ó Cofaigh, Department of Geography, as above.
Email: colm.ocofaigh@durham.ac.uk
†Present address: National Research Centre on Human Evolution (CENIEH), Burgos, Spain
[Correction added on 17 April 2021, after first online publication: Figures 3–9 were incorrectly ordered. This has been fixed now.]

(Chiverrell and Thomas, 2010; Clark *et al.*, 2012). The emerging picture is of an ice sheet that responded dynamically and sensitively to external climate and ocean forcing, but also one in which internal controls in the form of glacioisostatic depression, subglacial bed topography and sediment supply played an important role in triggering and/or modulating rates and patterns of ice sheet retreat (e.g. Eyles and Marshall McCabe, 1989; Chiverrell *et al.*, 2013; Small *et al.*, 2017; Ó Cofaigh *et al.*, 2019; Scourse *et al.*, 2019; Callard *et al.*, 2018, 2020; Van Landeghem and Chiverrell, 2020).

On the Atlantic shelf bordering west and northwest Ireland, previous work has documented glacial geomorphological and sedimentological evidence recording the advance and retreat of the BIIS across the continental shelf, typically to the shelf edge, during the Last Glacial Maximum (LGM) (Benetti *et al.*, 2010; Dunlop *et al.*, 2010; Ó Cofaigh *et al.*, 2012a, 2019; Callard *et al.*, 2018, 2020; Peters *et al.*, 2015, 2016, 2020; Roberts *et al.*, 2020; Craven *et al.*, 2021). These studies have shown that the ice sheet retreated in a glacimarine environment and radiocarbon dates on marine fauna in deglacial glacimarine sediments constrain the timing of this retreat. The term 'global Last Glacial Maximum' (gLGM) is used in this paper to refer to the period 26.5–19 ka when eustatic sea level was at a minimum because of global ice volume being at its highest (Clark *et al.*, 2009). The term 'local Last Glacial Maximum' (lLGM) refers to the period when specific ice sheets reached their maximum extent. The lLGM for the BIIS was attained at c. 27 ka (Clark *et al.*, 2012; Scourse *et al.*, 2019), and thus slightly earlier than the gLGM.

Working on the continental shelf west of Galway Bay, Peters *et al.* (2015, 2016) presented geomorphic and sedimentary evidence for extension of an ice lobe about 200 km westwards from the Irish mainland and onto the Porcupine Bank (Figs. 1 and 2), the outermost part of the Atlantic shelf bordering western Ireland. They dated this advance to sometime after 24.1 cal ka BP, hence during the LGM, and proposed that ice was grounded on the bank as late as 21.8 cal ka BP. Subsequently, however, Callard *et al.* (2020) presented sedimentological and radiocarbon data from the mid- and inner shelf which showed that initial retreat from Porcupine Bank was underway before 24.4 cal ka BP and that retreat across the mid-inner shelf was interrupted by oscillations or localized readvances of the ice sheet. These data constrained the age of a large composite grounding-zone wedge on the mid-shelf, variously termed the 'Mid-Shelf Grounding-Zone Complex' (Callard *et al.*, 2020) or the 'Galway Lobe Grounding-Zone Wedge' (Peters *et al.*, 2016), to c. ≤ 23 cal ka BP, with deglaciation of the shelf complete by about 17.1 cal ka BP. Earlier deglaciation of the inner shelf is, however, supported by terrestrial cosmogenic nuclide (TCN) dates on erratics of Galway granite from the Aran Islands (Fig. 2) which suggest that ice may have retreated from a marginal position at the mouth of Galway Bay (Fig. 2) by ~19.5 ka (Roberts *et al.*, 2020). TCN ages from around the Connemara (Fig. 2) coast of western Ireland indicate that ice margin retreat inland took place at 17.5–17.0 ka, suggesting that the ice sheet remained pinned on the Aran Islands/inner shelf for ~2–3 ka before retreating onshore (Roberts *et al.*, 2020).

Recent work on the shelf offshore of northwest Ireland and in the Malin Sea (Fig. 1) provides evidence for a shelf-edge terminating BIIS during the last glacial period, with initial retreat dated to 25.9 cal ka BP (Callard *et al.*, 2018) and > 24.8 cal ka BP (Ó Cofaigh *et al.*, 2019), and hence early in the gLGM. Ice sheet retreat across the shelf was driven by glacioisostatic depression and high relative sea level (RSL). Further south, the Irish Sea Ice Stream reached a maximum extent in the Celtic Sea (Fig. 1) at ~27 ka (Smedley *et al.*, 2017; Scourse *et al.*, 2019), during what was ostensibly an extensive, rapid and short-lived advance (Ó Cofaigh *et al.*, 2012b; Small *et al.*, 2018). Collectively this implies a difference of c. 3–4 ka between the timing of initial BIIS retreat offshore of central western Ireland (cf. Peters *et al.*, 2015, 2016), compared to the retreat of marine-based ice sheet outlets to the north and south.

In this paper we present new geophysical and dated sediment core records from the Porcupine Bank which provide insights into the extent and timing of BIIS advance and retreat on the Atlantic shelf west of Ireland during the LGM (Figs. 2–10). We then combine these new data with all previous geochronological data (Peters *et al.*, 2016; Callard *et al.*, 2020; Roberts *et al.*, 2020) in a Bayesian temporal model (Bronk Ramsey, 2009) to reconstruct the timing, pace and pattern of BIIS withdrawal across the shelf and adjacent coastline. The paper is the final synthesis of the BRITICE-CHRONO project for the Atlantic shelf sector west of Ireland.

Regional setting

The study area encompasses central western Ireland, and the adjoining continental shelf (Fig. 2). The mountains of Connemara form an area of rugged topography, incised by glacial troughs and corries. The mountains reach a maximum elevation of 814 m and are mostly composed of quartzite with some schist or gneiss. They are separated from the coast by an extensive area of lowland topography developed chiefly on the Caledonian Galway granite (Davies and Stephens, 1978). To the south of Galway Bay, in County Clare (Fig. 2), the topography is developed on Carboniferous limestone and Namurian sandstones and shales. The limestone area of north County Clare comprises the karstic region known as the 'Burren' (derived from the Irish word 'Boireann' meaning rocky ground). The three Aran Islands at the mouth of Galway Bay (Fig. 2) form the offshore extension of the limestone terrain of the Burren.

The continental shelf extends for about 150 km westwards from the present coastline to the Slyne Trough (sometimes referred to as the Porcupine Saddle) which separates the

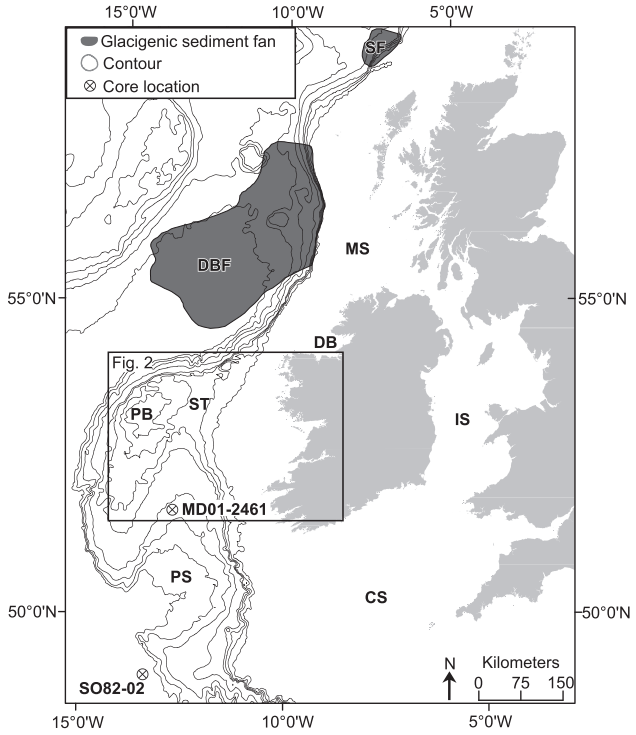

Figure 1. Location of the study area in the context of Ireland and Britain, as well as locations referred to in the text. IS = Irish Sea, CS = Celtic Sea, MS = Malin Sea, DB = Donegal Bay, PB = Porcupine Bank, ST = Slyne Trough, PS = Porcupine Seabight, DBF = Donegal-Barra Fan. SF = Sula Sgeir Fan. Location of Fig. 2 is outlined.

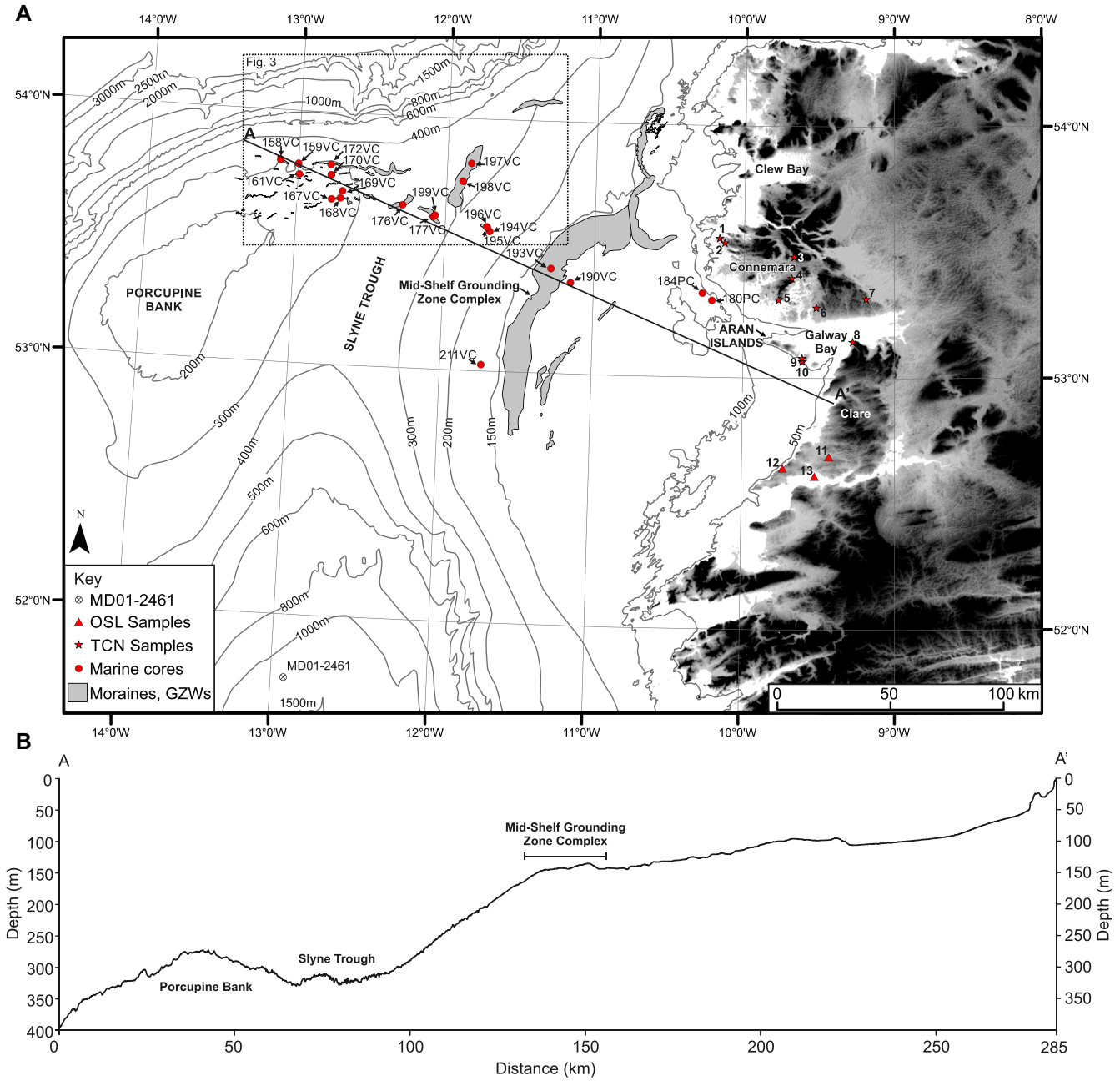

Figure 2. Location map of the study area showing central western Ireland and the adjoining continental shelf. (A) Shelf bathymetry, location of moraines and grounding-zone wedges on the shelf, as well as the location of radiocarbon-dated marine sediment cores and terrestrial OSL- and TCN-dated sample sites (see Tables, 1, 2, 3 and 4). The location of the bathymetric profile A–A′ shown in panel B is also indicated. The main Irish shelf is separated from the shallow Porcupine Bank by the bathymetric deep of the Slyne Trough. (B) Bathymetric profile extending from offshore of the present coastline to the continental shelf edge west of Porcupine Bank. The location of the 'Mid-shelf Grounding Zone Complex' is shown. [Color figure can be viewed at wileyonlinelibrary.com]

mid-shelf from the Porcupine Bank to the west. The Slyne Trough is approximately 70 km wide and reaches water depths of > 300 m. Water depths across the inner to mid-shelf are < 200 m. The inner shelf is underlain by an offshore extension of the Precambrian metasedimentary rocks of Connemara and the Carboniferous limestone of the Clare Basin (Naylor *et al.*, 1999), overlain in turn by Pliocene and Quaternary sediments.

The Porcupine Bank forms the outermost part of the continental shelf west of Ireland between 51–54°N and 11–15°W. It is located approximately between 150 and 250 km from the Irish coastline and covers an area of more than 40 700 km^2. It is the westwards projection of the main Irish continental shelf to which it is linked by the Slyne Trough. The Porcupine Bank itself comprises a north–south-trending plateau and is the north-western margin of the Porcupine Seabight Basin (Naylor and Shannon, 2009). Water depths across the bank are typically 200–400 m (Thébaudeau *et al.*, 2016). The SW–NE-orientated Porcupine Ridge in the north forms the shallowest area with water depths of < 200 m, and the shallowest point on the bank overall is 145 m (Thébaudeau *et al.*, 2016). Along the northern and western sides of the bank the shelf break occurs at c. 400 m water depth and the continental slope is steep (Sacchetti *et al.*, 2012). This contrasts with the southern Porcupine Bank where it slopes gently down into the Porcupine Seabight (Fig. 1). Slope gradients over most of the bank are generally < 0.5° (Thébaudeau *et al.*, 2016).

Methods

Multibeam bathymetric data were collected by the Geological Survey of Ireland and the Irish Marine Institute during cruises of

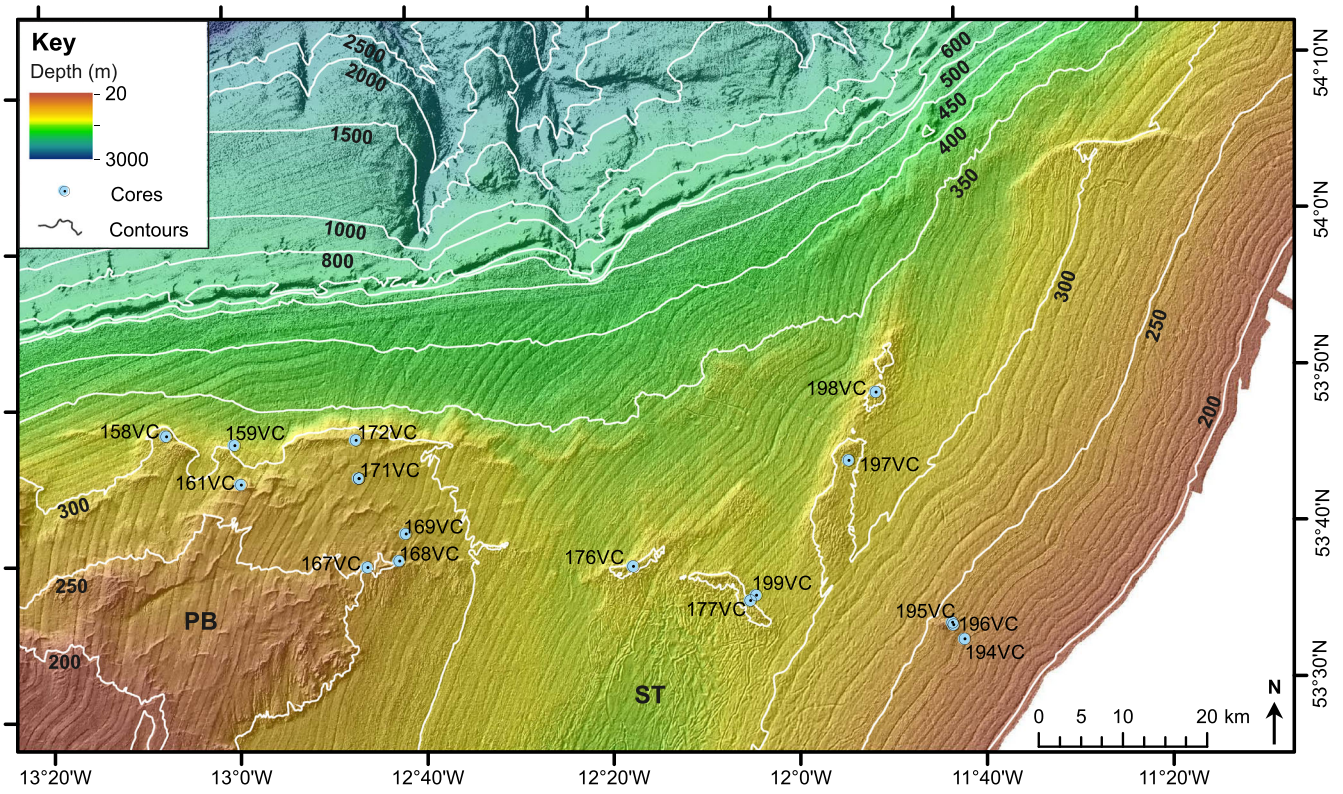

Figure 3. Colour-shaded relief bathymetric image of the seafloor of the mid-outer western Irish shelf and Porcupine Bank. Bathymetric contours and sediment cores referred to in the text are shown. Data source: INFOMAR (Integrated Mapping for the Sustainable Development of Ireland's Marine Resource; Geological Survey of Ireland and Marine Institute). [Color figure can be viewed at wileyonlinelibrary.com]

the *RSV Siren* in 2000 and 2001 as part of the Irish National Seabed Survey (INSS) and Integrated Mapping for the Sustainable Development of Ireland's Marine Resource (INFOMAR) programmes. The bathymetric data were collected using a hull-mounted Simrad EM1002 multibeam system. They provide a geomorphological context for the new seismic records, sediment cores and dating results that we discuss in this paper. The multibeam system has an operational frequency of 93–98 kHz, pulse lengths of 0.5 ms (150–250 m) and 0.7 ms (250–500 m), and decimetric vertical and horizontal accuracy of 50 cm or better according to water depth (Thébaudeau *et al.*, 2016). Data were gridded at a cell size of 25 m. Linear data artefacts are visible at the edges of overlapping survey lines across the study area. Their visual effect was minimized using a range of different sun-illumination angles (Thébaudeau *et al.*, 2016).

New information on acoustic stratigraphy and sediment thickness were acquired during cruise JC106 of the *RRS James Cook* in 2014 using a hull-mounted Kongsberg SBP120 sub-bottom profiler. The SBP120 system uses a transducer with a frequency sweep range of 2.5–7 kHz installed as part of the EM120 wideband receiver array. It has a typical maximum penetration depth of 50 m (depending on the nature of the sediments) and a nominal depth resolution of 0.3 ms. Two-way travel times in seconds were converted to depth below sea level at the time of surveying using typical values of sound velocity (1500 m s^{-1} through the water column and 1600 m s^{-1} through soft sediments). The data were visualized in IHS Kingdom.

Sediment cores were collected from across the Porcupine Bank using a 6-m-long British Geological Survey vibrocorer during cruise JC106 (Figs. 2, 3, 8 and 9; Table 1). Core sites were selected to target glacigenic seafloor landforms, particularly grounding-zone wedges. Following collection, the sediment cores were cut into 1-m-long sections, split, and information recorded on grain size, sedimentary and deformation structures, sorting, colour, the nature of bedding contacts, clast abundance and shape, and macrofaunal content. Measurement of sediment shear strength in kPa was recorded using a Torvane. Magnetic susceptibility and wet bulk density were measured on-board during cruise JC106 using a GEOTEK multi-sensor core logger (MSCL). Post-cruise, the cores were X-rayed using a GEOTEK MSCL-XCT scanner to obtain additional information on sedimentary structures. The cores were stored on ship and subsequently in Durham University at 4 °C.

Samples of marine molluscs (typically single or broken valves) and benthic foraminifera were collected for radiocarbon dating (Table 2). Samples typically targeted subglacial to deglacial lithofacies boundaries or, where cores bottomed out in deglacial sediment, the base of the core to obtain a minimum age constraint on ice sheet retreat. In addition, individual reworked shells from subglacial till were dated to provide a maximum age on till formation and thus ice sheet advance.

The radiocarbon dates were corrected for isotopic fractionation and then calibrated using the Marine13 calibration curve that incorporates a standard marine reservoir effect of 400 years. Delta-R values of 0, 300 and 700 years were then also applied. The radiocarbon and calibrated ages with Delta-R values of 0, 300 and 700 years are presented in Table 2. However, only those ages calibrated with a Delta-R of 0 years are used in the text due to spatial and temporal uncertainties in the radiocarbon reservoir ages in the North Atlantic and adjoining continental shelves since the LGM (cf. Wanamaker *et al.*, 2012).

A Bayesian temporal model implemented using OxCal 4.3 (Bronk Ramsey, 2009) was used to analyse the geochronological data and so reconstruct the pattern of deglaciation. The Bayesian modelling follows that described in Chiverrell *et al.* (2018). The Bayesian approach allows us to integrate different types of chronological data [radiocarbon, TCN and optically stimulated luminescence (OSL); Tables 2, 3 and 4] and to

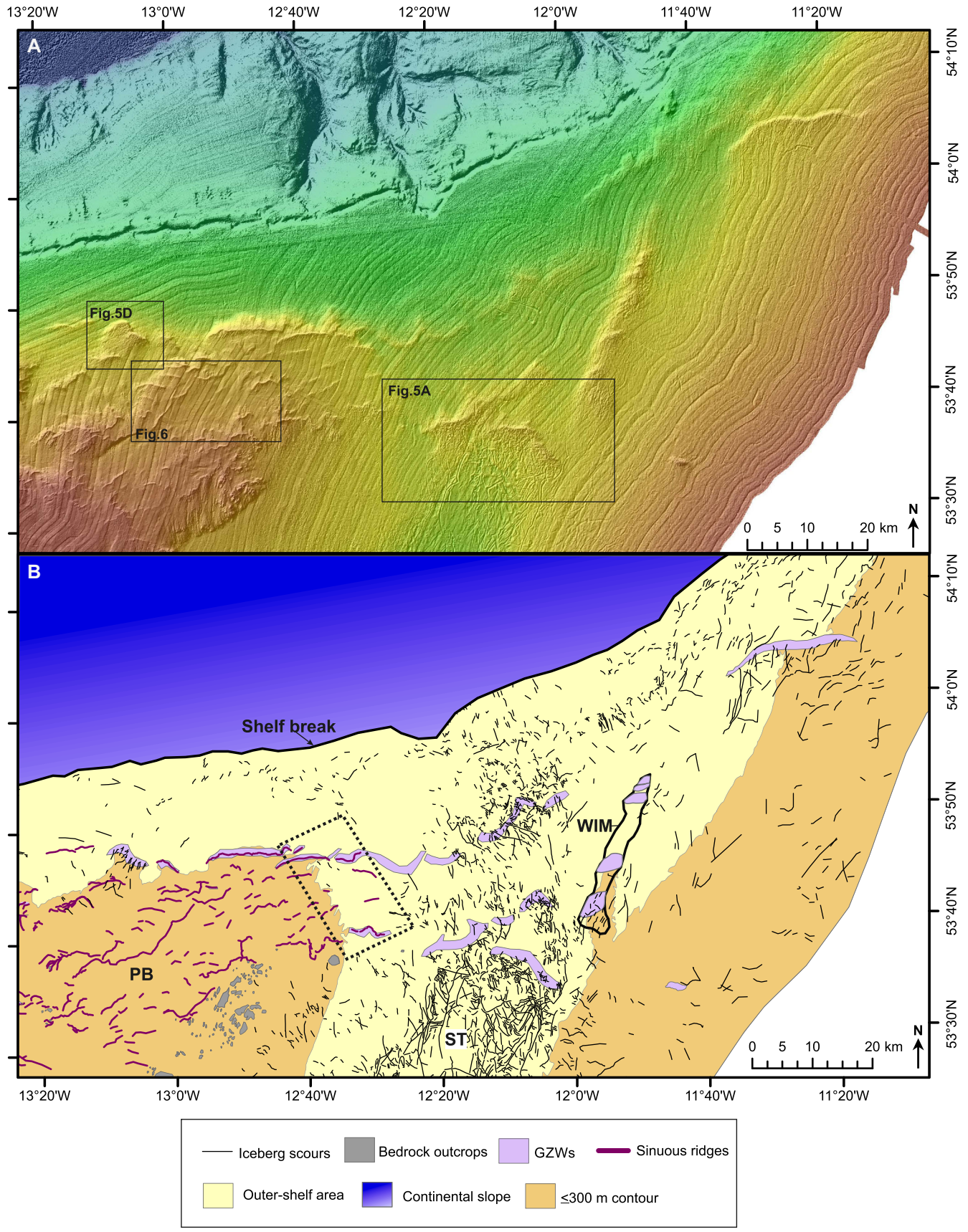

Figure 4. Glacial geomorphology of the western Irish shelf and Porcupine Bank as mapped from multibeam swath bathymetric data. Source: INFOMAR (Integrated Mapping for the Sustainable Development of Ireland's Marine Resource; Geological Survey of Ireland and Marine Institute). (A) Colour-shaded relief bathymetric image of the seafloor of the mid-outer western Irish shelf and Porcupine Bank showing location of subsequent figures; (B) mapped geomorphology of the seafloor shown in panel A and modified from Thébaudeau *et al.* (2016). PB = Porcupine Bank, ST = Slyne Trough, WIM = West Ireland Moraine. The dashed box outlines the zone where moraines on the Porcupine Bank transition with increasing water depth into grounding-wedges in the Slyne Trough. [Color figure can be viewed at wileyonlinelibrary.com]

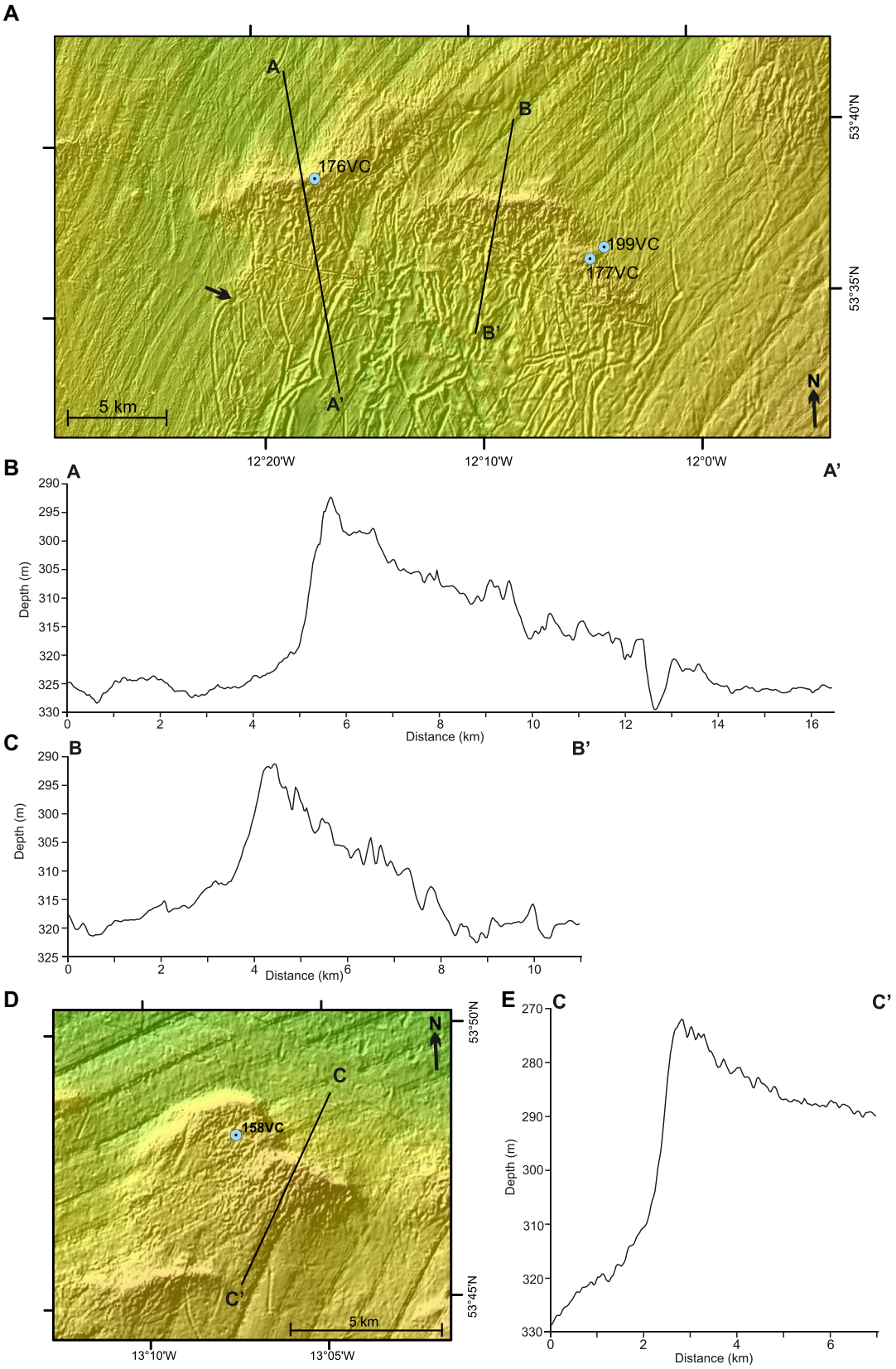

Figure 5. Details of grounding-zone wedges in the Slyne Trough and outer Porcupine Bank showing their seafloor morphology in plan-view and associated topographic profiles. Locations shown in Fig. 4. Note the characteristic 'ramp-step' form of the grounding-zone wedges and the heavily iceberg-furrowed ramp slopes. (A) Colour-shaded relief bathymetric image of grounding-zone wedges in the Slyne Trough. The arrow marks the location of a crudely circular depression, interpreted as an iceberg wallow pit, which occurs the end of a curvilinear iceberg furrow. (B,C) Topographic profiles across the grounding-zone wedges shown in A. (D) Colour-shaded relief bathymetric image of grounding-zone wedge on outer Porcupine Bank from which core 158VC was recovered. The core site location is shown on the image. (E) Topographic profile across the grounding-zone wedge shown in D. Data source for the multibeam imagery: INFOMAR (Integrated Mapping for the Sustainable Development of Ireland's Marine Resource; Geological Survey of Ireland and Marine Institute). [Color figure can be viewed at wileyonlinelibrary.com]

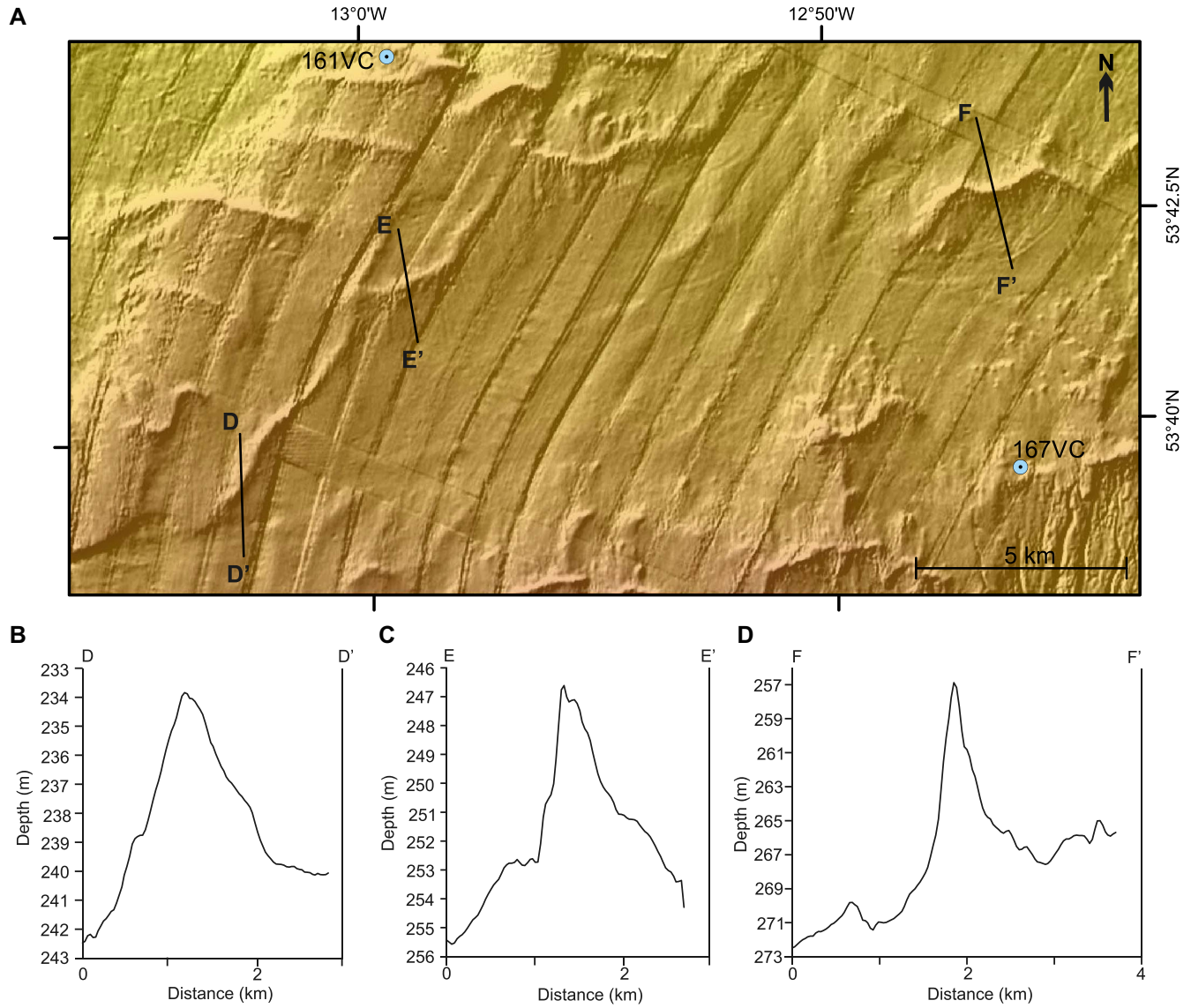

Figure 6. Detail of sharp-crested sinuous ridges interpreted as moraines on the Porcupine Bank showing their seafloor morphology in plan-view and associated topographic profiles. Location shown in Fig. 4. Note the contrast in morphology with the grounding-zone wedges shown in Fig. 5. Data source for the multibeam imagery: INFOMAR (Integrated Mapping for the Sustainable Development of Ireland's Marine Resource; Geological Survey of Ireland and Marine Institute). [Color figure can be viewed at wileyonlinelibrary.com]

identify data outliers. It uses a 'prior model' (the order of events) to refine probability distributions when presented as a relative order of events (Chiverrell *et al.*, 2013, 2018). The prior model is constructed using the events or ice-marginal positions interpreted from the geomorphological and stratigraphic evidence, and arranged in the order of ice retreat, determined independently of the geochronological data. The Bayesian analysis then uses this prior model to assess the possibility of outliers but does not automatically reject these depending on the landform and/or stratigraphic context or the measurement. The approach uses the relationship between dated sites [grounding-zone wedges (GZWs), moraines, core sites and sediment exposures, as well as erratic boulders and ice-moulded bedrock], and the modelling can reduce the uncertainty ranges for individual age estimates (Bronk Ramsey, 2009; Chiverrell *et al.*, 2018). The individual age measurements (radiocarbon, TCN, OSL; Tables, 2, 3 and 4) are expressed as age probability functions that represent the likelihood that any one sample has a particular age (Bronk Ramsey, 2009).

To explore the timing of ice margin retreat, the age control within our prior model has been divided into a series of Phases, each representing the geochronology either for specific sites or zones of the former ice mass. Each Phase, in the Bayesian terminology (Bronk Ramsey, 2009), contains grouped dating information that shares a common relationship with other items in the prior model, and they are separated by Boundaries that delimit the period of each Phase (Fig. 11). The Boundary command in the software generates modelled age estimates that are then used to define the timing of ice margin retreat. The modelling uses Markov chain Monte Carlo sampling to build up a distribution of possible solutions. For each sample it generates a probability called a posterior density estimate which is the product of both the prior model and the likelihood probabilities. This approach generated modelled ages for boundaries in the prior model that separate a series of ice retreat zones, with each zone coded as a Phase. The sequence model was run in an outlier mode to assess for outliers in time. The Bayesian analysis produced a conformable age model for ice sheet retreat on the shelf offshore of western Ireland with an overall agreement index of 136%, thus exceeding the > 60% threshold advocated by Bronk Ramsey (2009).

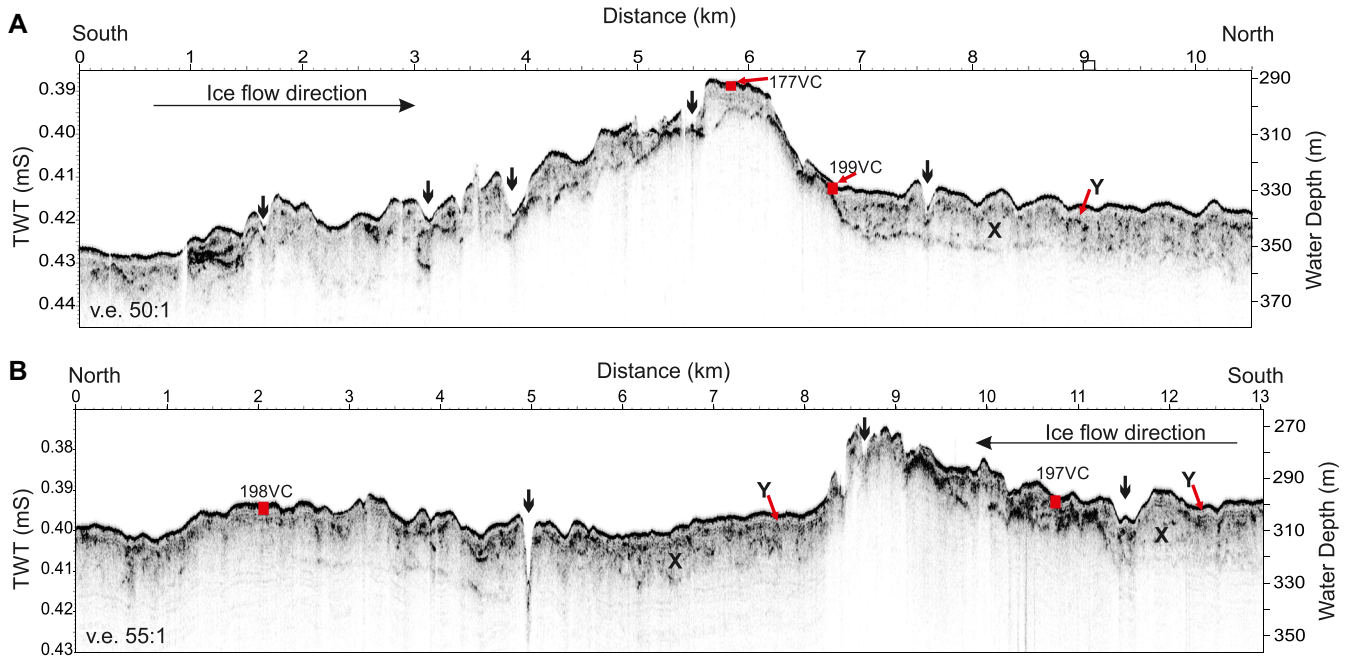

Figure 7. Representative sub-bottom profiles of grounding-zone wedges (GZWs) from the study area showing the internal acoustic stratigraphy. Locations of sediment cores discussed in the text are also shown. (A) GZW from the outer Slyne Trough shown in Fig. 5A as profile line B–B′. Note the heavily iceberg-furrowed surface of the GZW; prominent iceberg furrows are arrowed. (B) Back-stepping GZWs on the surface of the West Ireland Moraine from the eastern side of the Slyne Trough (See Fig. 4B). Prominent iceberg furrows are arrowed. Both profiles show the presence of two acoustic stratigraphic units labelled 'X' and 'Y'. The lower unit X is acoustically homogeneous and overlies a diffuse to locally strong and irregular basal reflector. The upper unit Y is a conformable sediment drape that is commonly acoustically transparent internally. [Color figure can be viewed at wileyonlinelibrary.com]

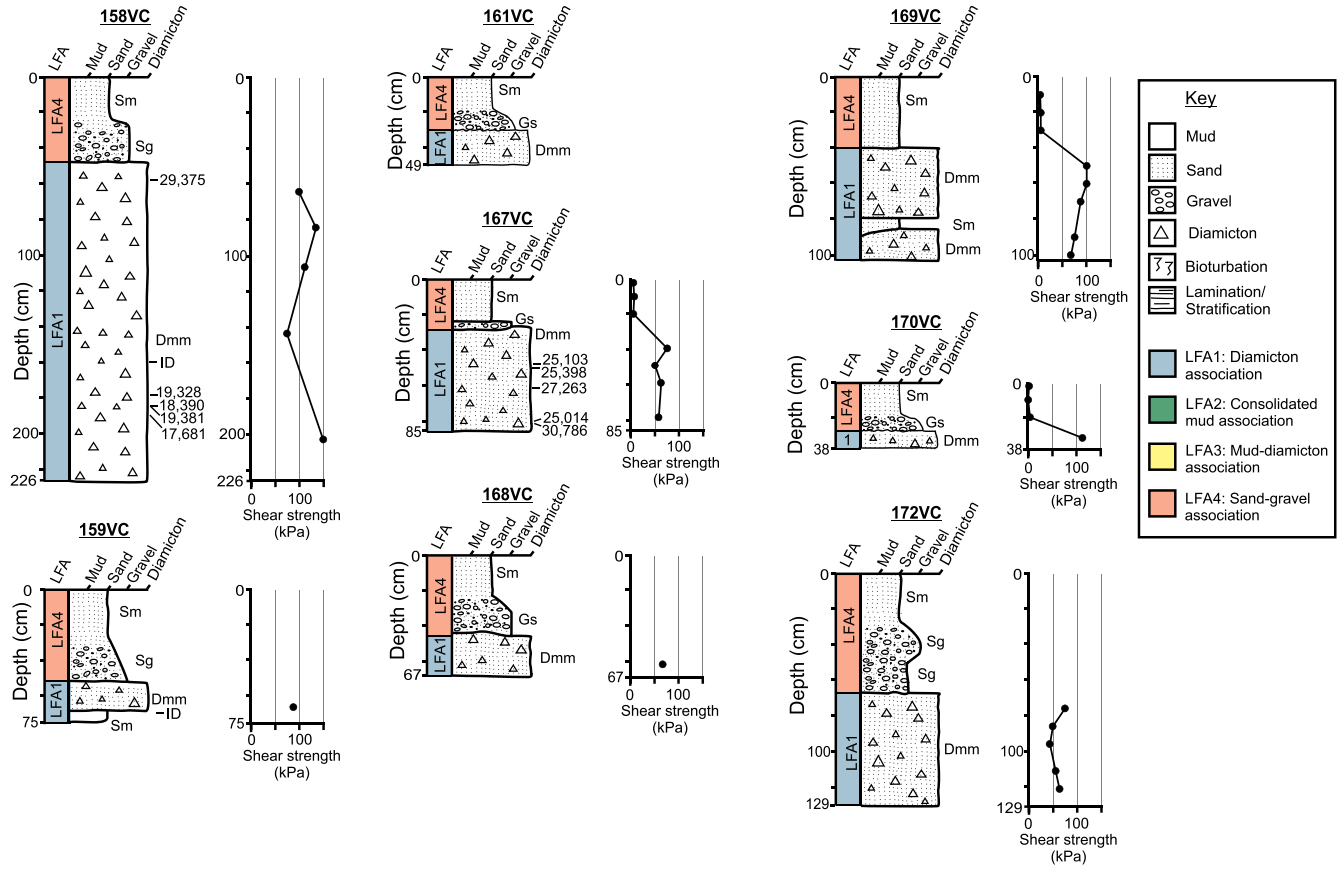

Figure 8. Lithofacies logs, associated shear strength measurements in kPa and calibrated radiocarbon dates from sediment cores from the Porcupine Bank. 'ID' refers to radiocarbon dates that were indistinguishable from background. Lithofacies codes are shown and 'LFA' refers to the lithofacies associations discussed in the text with the different LFAs colour-coded for ease of identification. Sediment core locations are shown in Figs. 2 and 3. [Color figure can be viewed at wileyonlinelibrary.com]

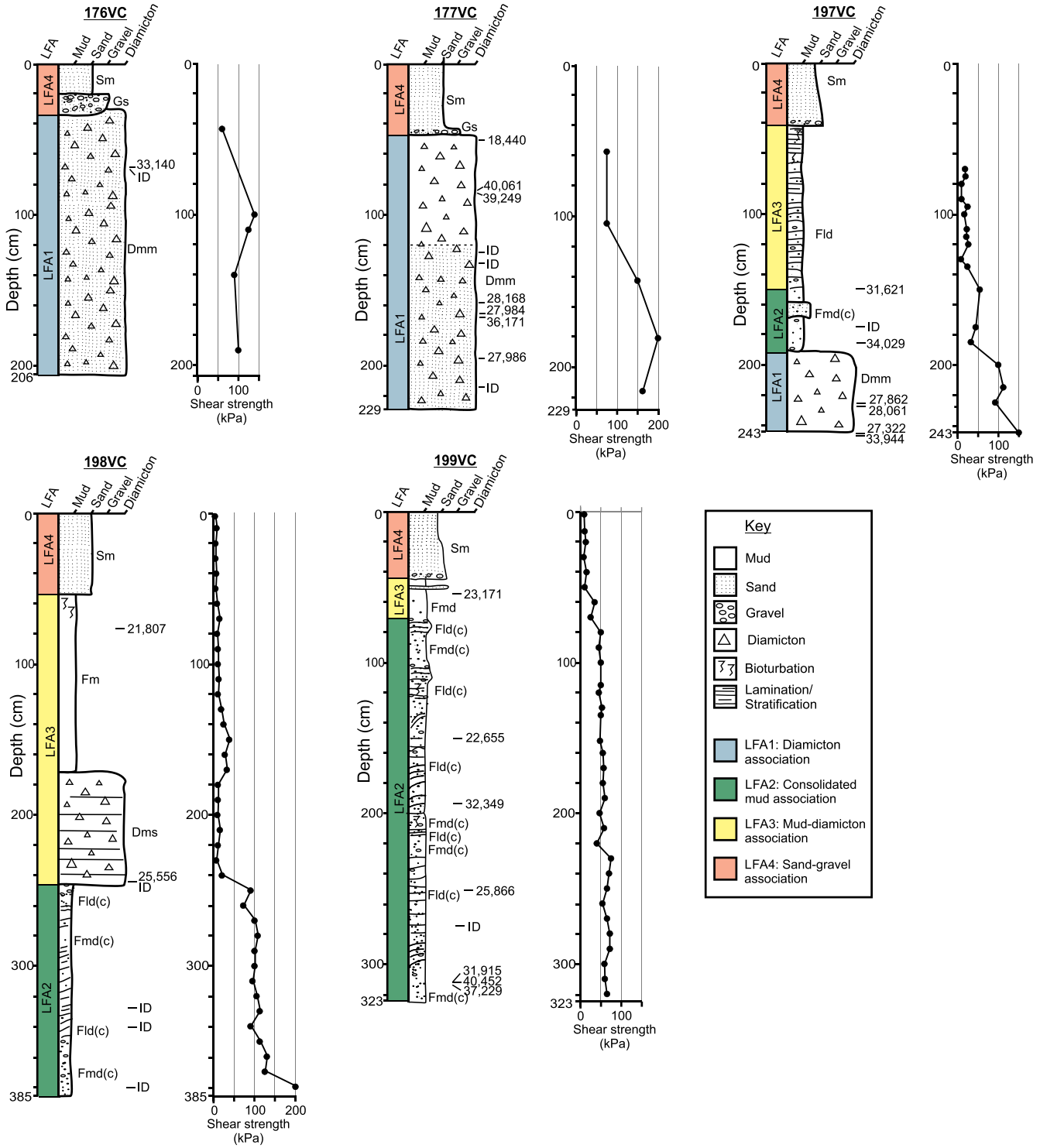

Figure 9. Lithofacies logs, associated shear strength measurements in kPa and calibrated radiocarbon dates from sediment cores from the Slyne Trough. 'ID' refers to radiocarbon dates that were indistinguishable from background. Lithofacies codes are shown and 'LFA' refers to the lithofacies associations discussed in the text, with the different LFAs colour-coded for ease of identification. Sediment core locations are shown in Figs. 2 and 3. [Color figure can be viewed at wileyonlinelibrary.com]

Results and interpretations

Seafloor geomorphology and acoustic stratigraphy

We use the detailed description of the seabed geomorphology of the Porcupine Bank and Slyne Trough by Thébaudeau *et al.* (2016), concentrating on the northern sector of the Porcupine Bank, including the outer shelf, and the Slyne Trough. We describe new acoustic stratigraphic data from these areas and discuss their origin and significance in terms of ice sheet advance and retreat.

A series of prominent ridges extend across the Slyne Trough and Porcupine Bank (Figs. 3–7). These ridges are generally orientated east to west and north-east to south-west although there is some variability. We distinguish two characteristic forms: wedges and sharper, locally sinuous, ridges. The wedges occur within the Slyne Trough and across the outer shelf of the northern bank. They are typically characterized by a well-defined asymmetrical ramp-scarp form with a steeper north-facing slope or scarp (up to 3°) and a gentler southern slope or ramp (up to 1.5°) (Figs. 4, 5 and 7). They range from

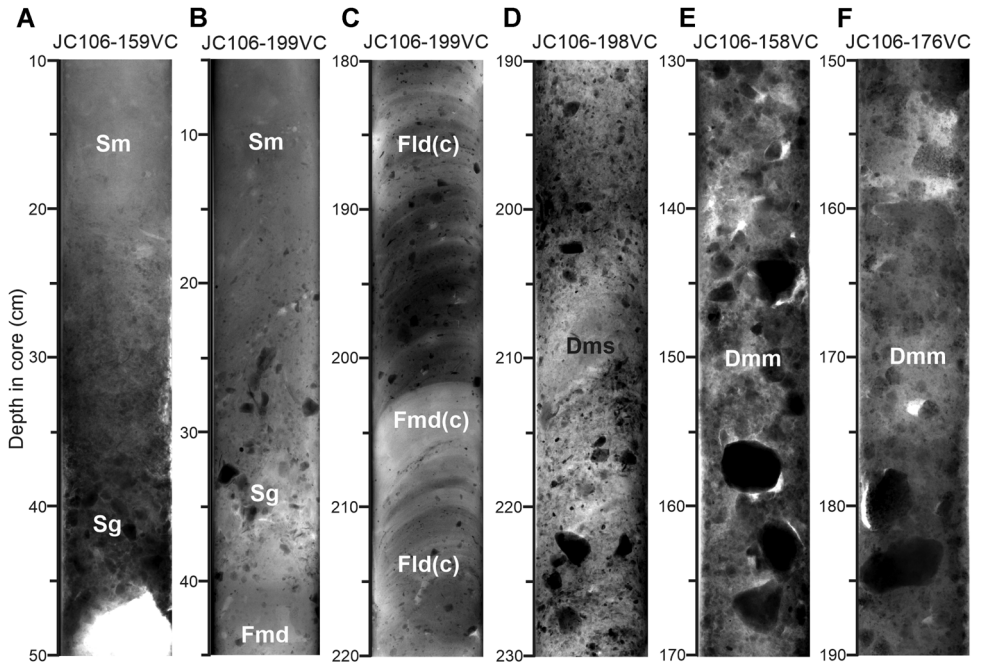

Figure 10. X-radiographs showing details of lithofacies from the study area. See Figs. 2 and 3 for core locations. (A) Facies Sg-Sm (LFA4). Fining-upwards gravelly sand (LF8) overlain gradationally by massive sand (LF9). Core 159VC, 50–10 cm depth. (B) Facies Sg-Sm (LFA4). Crudely fining-upwards gravelly sand (LF8) and massive sand (LF9) overlying facies Fmd (LF6). Core 199VC, 45–0 cm. (C) Facies Fld(c) and Fmd(c) (LFA2). Consolidated and laminated (LF3) and massive (LF4) mud with clasts. Core 199VC, 220–180 cm depth. (D) Facies Dms (LFA3). Stratified, matrix-supported diamicton (LF2). Core 198VC, 230–190 cm depth. (E) Facies Dmm (LFA1). Massive, matrix-supported diamicton (LF1). Core 158VC, 170–130 cm depth. (F) Facies Dmm (LFA1). Massive, matrix-supported diamicton (LF1). Core 176VC, 190–150 cm depth.

5 to 30 m in height and are up to 20 km long (across-trough). In planform they are curvilinear to locally arcuate. Although the distribution of wedges is discontinuous across the Porcupine Bank and Slyne Trough, an outer shelf set, located ~15 km inshore of the shelf break, can be distinguished as well as a series of back-stepping wedges to the south and east (Fig. 4). On the eastern side of the Slyne Trough back-stepping, east–west-orientated wedges up to 15 m high can be seen to overprint a much larger ridge orientated NNE–SSW (Figs. 4 and 7B). Cores from these wedges confirmed that they are composed of sediment (see below 'Sedimentology and radiocarbon measurements' and Fig. 9).

Sub-bottom profiles from across the wedges show a clear asymmetrical, ramp–scarp form with the steeper scarp face on the north side (Figs. 5 and 7). Sediment thicknesses across the wedges range from 1 to 10 m and are thickest on the southern (ramp) slope and at the base of the frontal scarp faces. The profiles show the presence of two acoustic units: a lower acoustically homogeneous unit, up to c. 20 m thick, that overlies a diffuse to locally strong and irregular basal reflector, and an overlying 3–5 m of conformably draped sediment (Fig. 7). Internally, the drape is often acoustically transparent but occasionally is diffusely stratified; the wedges are transparent and no internal structure was observed. A characteristic feature of the wedges is that they are incised by furrows which can be up to 10 m deep (Figs. 5 and 7). Furrows are particularly well developed on the wedge crests and ramp slopes, and in places incise both stratigraphic units.

Across the northern Porcupine Bank a series of sharp-crested, locally sinuous or crenulated ridges are visible (Figs. 4 and 6). The ridges are narrow and typically 2–3 km wide, up to c. 6 km long and up to a maximum of 14 m high above the surrounding seafloor. Similar to the wedges, these narrower ridges are discontinuous but the individual segments appear to align. The ridges occur predominantly in water depths shallower than c. 300–330 m, below which they transition to wedges (Fig. 4). The internal structure of the ridges could not be resolved in detail due to low acoustic penetration. The acoustic stratigraphy is limited to c. 7 m of sediment comprising a lower unit that is semi-transparent to homogenous with a localized distribution. This is overlain by a more continuous, homogenous unit, with a high-amplitude seabed reflector. Sediment cores from these ridges bottomed out in stiff, sandy, matrix-supported massive diamicton (see below).

Thébaudeau *et al.* (2016) mapped over 30 000 cross-cutting furrows across the study area. The furrows occur in water depths of 180–575 m and two main orientations are recorded: south to north and east to west. In form, the furrows are linear to curvilinear, up to 300 m wide, 10 m deep and 20 km long. Some of the furrows are bounded by 1–2 m-high berms, either singly or paired. Thébaudeau *et al.* also described craters or pits up to 15 m deep which occur at one end of individual furrows (e.g. Fig. 5A). As noted above, furrows incise the wedges, and are particularly well developed on the southern (ramp) slope and crest (Figs. 5 and 7).

Interpretation

Sediment cores confirm that both the ridges and wedges are composed of sediment. The size and morphology of the wedges within the Slyne Trough and across the northern Porcupine Bank are consistent with descriptions of GZWs from glaciated continental shelves (e.g. Evans *et al.*, 2005; Ó Cofaigh *et al.*, 2005; Dowdeswell and Fugelli, 2012). This interpretation is based on their asymmetrical ramp–scarp form and, in planform, their curvilinear to arcuate expression on the seafloor. The sharp-crested sediment ridges are narrower than the GZWs and on this basis are interpreted as ice-marginal moraines (Bradwell *et al.*, 2008; Ottesen and Dowdeswell, 2009; Ó Cofaigh *et al.*, 2012a; Batchelor and Dowdeswell, 2015). GZWs are usually inferred to represent formation in a sub-ice shelf cavity where vertical accretion is constrained, thereby producing the ramped form, whereas sharp-crested moraines are commonly inferred to form at a

grounded, tidewater ice margin (Batchelor and Dowdeswell, 2015; Smith *et al.*, 2019). Across the Slyne Trough and Porcupine Bank GZWs occur predominantly in water depths greater than *c.* 300–330, whereas the moraines occur in shallower water (Fig. 4). This pattern may reflect a transition from an ice shelf within the deeper water of the Slyne Trough to a grounded (tidewater) margin across the shallower bank.

The back-stepping pattern of the moraines and GZWs indicates that grounding-line retreat across the outer Porcupine Bank was episodic and was characterized by periodic stillstands or oscillations (cf. Dowdeswell *et al.*, 2008; Ó Cofaigh *et al.*, 2008). Oscillatory behaviour is suggested by the arcuate and locally crenulate or sinuous form of the GZWs and moraines (cf. Bradwell *et al.*, 2008). The back-stepping east–west-orientated GZWs that overprint the large NNE–SSW ridge on the east side of the Slyne Trough (Fig. 4) postdate that ridge as they are formed on top of it and they also align with GZWs further to the west. Peters *et al.* (2016) termed the larger ridge the 'West Ireland Moraine' (Fig. 4B) and inferred that this represented a push moraine that was ornamented with smaller superimposed GZWs built by a grounding ice shelf during extension over the Slyne Trough.

The acoustically homogeneous to transparent facies that makes up the cores of the GZWs and moraines is similar to previous observations of these landforms from high-latitude continental margins (e.g. Shipp *et al.*, 1999, 2002; Evans *et al.*, 2005; Hogan *et al.*, 2012; Batchelor and Dowdeswell, 2015). This acoustic facies is interpreted as a diamicton probably sourced from a subglacial deforming layer that was advected to the grounding line (cf. Ó Cofaigh *et al.*, 2005, 2007; Evans *et al.*, 2009). Subsequent deposition of this diamicton formed a subglacial traction till, although it is likely that it was also at least partly produced by sediment reworking, either through glacitectonism during minor fluctuations of the grounding line and/or through debris flow processes (cf. Hogan *et al.*, 2016; Evans, 2018). The presence of subglacial till is consistent with sediment cores which bottomed out in stiff, matrix-supported diamicton (see 'Sedimentology and radiocarbon measurements' below). The acoustic drape which overlies the GZWs is inferred to be a product of formation in a deglacial and/or postglacial environment by passive suspension settling of fine-grained sediment through the water column.

Cross-cutting, linear to curvilinear furrows with paired or single lateral berms which incise the surfaces of the GZWs and occur across much of the study area (Thébaudeau *et al.*, 2016) are interpreted to be iceberg ploughmarks, produced by the intermittent scouring of grounded iceberg keels in contact with the seafloor (e.g. Woodworth-Lynas *et al.*, 1991; Dorschel *et al.*, 2010; Sacchetti *et al.*, 2012). The associated craters, which occur at furrow ends, are probably 'iceberg wallow' structures related to the stranding of icebergs (cf. Reimnitz and Kempema, 1982; Longva and Bakkejord, 1990; Stewart *et al.*, 2016). An alternative interpretation for furrows on the ramp slopes of the GZWs is that they were formed by erosion by irregularly shaped ice keels at the base of an ice shelf in the transition zone from grounded to floating ice (e.g. Graham *et al.*, 2010). However, such features typically exhibit high linearity and can terminate abruptly at an asymmetrical mound (Smith *et al.*, 2019). This is at odds with the marked curvilinear form of many of these features on the Porcupine Bank GZWs and their termination in depressions or pits at one end. Hence an interpretation of iceberg ploughmarks is preferred.

Sedimentology and radiocarbon measurements

Sixteen vibrocores, targeting sediment ridges interpreted as GZWs and moraines on the Porcupine Bank and in the Slyne Trough, were investigated in this study (Figs. 2, 3, 8 and 9). Nine lithofacies are identified based on core lithology, sedimentary structures and physical property measurements. These lithofacies are described below along with dating constraints. Core logs and stratigraphic positions of the dates are shown in Figs. 8 and 9, as well as in Supplementary Information figures a and b. Figure 10 shows x-radiograph examples of the various lithofacies.

Lithofacies 1. Massive, matrix-supported diamicton (Dmm)

This lithofacies comprises a massive, matrix-supported, dark grey (5Y4/1) diamicton that typically forms the basal lithofacies in cores from the Porcupine Bank (Figs. 8 and 10). The matrix ranges from sandy (e.g. cores 167VC, 176VC) to muddy (e.g. cores 158VC, 177VC) in texture. Clasts from within the diamicton matrix are rounded to sub-angular and are granule to pebble in size. Clast abundance is variable and, as a result, the diamicton ranges from quite clast-rich and gravelly (e.g. 158VC), to more matrix-rich in which small clasts are dispersed throughout the matrix (e.g. 197VC). There is no discernible internal structure, either visually or within the X-radiographs (Figs. 8–10). The diamicton is characteristically stiff with shear strengths ranging from 33 to 200 kPa and averaging 100 kPa. The wet bulk density is also high, averaging 2.3 g ml^{-1} (Supplementary Information Figs. a and b). The upper boundary is predominantly sharp, and occasionally convoluted. Magnetic susceptibility varies within and between cores, averaging 502 SI. However, this high value is biased by core 176VC that has values consistently above 1300 SI and when it is removed from calculation the average magnetic susceptibility reduces to 214 SI (Supplementary Information Figs. a and b).

The age of the Dmm facies is constrained by 29 radiocarbon measurements on shell and coral fragments that were sampled from cores 158VC, 159VC, 167VC, 176VC, 177VC and 197VC (Figs. 8 and 9; Table 2). Of these, seven were indistinguishable from background. Most of the ages are between 36.2 and 25.0 cal ka BP. The youngest ages in this group, 25 510 ± 265 (SUERC-58389), 25 398 ± 206 (SUERC-67932) and 25 014 ± 310 (SUERC-67937) cal a BP, are all from core 167VC. Two cores contain samples which yielded considerably younger ages. An age of 18 440 ± 145 (SUERC-68872) cal a BP was obtained from an articulated bivalve of *Yodiella* species towards the top of the diamicton in core 177VC. Core 158VC contains several relatively young ages which occur in reverse stratigraphic order and are, from deepest to shallowest, 17 681 ± 184 (SUERC-63582), 19 381 ± 174 (SUERC-67931), 18 390 ± 157 (SUERC-67930), 19 328 ± 186 (SUERC-63578) and 29 375 ± 284 (SUERC-63577) cal a BP (Fig. 8).

Lithofacies 2. Stratified, matrix-supported diamicton (Dms)

This facies is only observed from 246 to 173 cm depth in core 198VC (Figs. 9 and 10). Stratification is inclined and is imparted by textural banding in which zones of diamicton are interbedded with more silty horizons. The stratification is particularly well developed in the lowermost 30 cm, becoming more diffuse gradationally above. Individual beds are internally massive. The lower contact of this facies is gradational although shear strength shows an abrupt decrease across this transition dropping from 90 kPa at 250 cm depth to 20 kPa at 240 cm. Shear strength through the Dms ranges from 6 to 20 kPa. The upper contact is sharp. Two samples from the close to the base of the Dms were radiocarbon dated to provide age constraint on the timing of formation (Fig. 9; Table 2).

A sample of mixed benthic foraminifera from 243 cm depth gave a non-finite age (SUERC-63563). A second sample from 244 cm depth of monospecific *Elphidium clavatum* dated to 25 556 + 237 (UCIAMS-176368) cal a BP.

Lithofacies 3. Laminated mud, consolidated (Fld(c))

This facies is identified in three cores, 197VC, 198VC and 199VC. It is a dark grey (5Y4/1) to olive grey (5Y4/2) laminated clayey silt that contains dispersed granules and occasional pebbles as well as abundant, dispersed shell and coral fragments. Laminations vary from inclined to horizontal and have variably sharp or diffuse upper and lower contacts. In core 197VC the laminations become distorted towards the top of this unit and contain a deformed, 9-cm-thick, grey (5YR5/1) silt bed at 159–168 cm (Fig. 9). The shear strength of this facies ranges from 33 to 112 kPa, with an average of 80 kPa. Both the magnetic susceptibility and the wet bulk density are also relatively high and are 99 SI and 2.02 g ml^{-1}, respectively (Supplementary Information Figure b). Seven radiocarbon ages were obtained from this lithofacies (Fig. 9; Table 2). The youngest, a monospecific *Elphidium clavatum* sample collected from 152 cm in core 199VC, yielded an age of 22 655 ± 221 cal a BP (UCIAMS-176369). A second monospecific *E. clavatum* sample from 248 cm depth in 199VC produced an age of 25 886 ± 221 cal a BP (UCIAMS-186911) while a shell fragment from 275 cm in the same core was indistinguishable from background. Two shell fragments at 150 and 185 cm in core 197VC yielded ages of 31 621 ± 347 (SUERC-60173) and 34 029 ± 270 cal a BP (SUERC-63583), respectively. A further two shell fragments from core 198VC produced ages that were indistinguishable from background.

Lithofacies 4. Massive mud with clasts, consolidated (Fmd(c))

This facies occurs in cores 198VC and 199VC where it is the basal facies in both cores (Fig. 9). It consists of a dark grey to olive-grey (5YR4/1–5YR4/2), massive, silty clay with dispersed, predominantly granule-sized clasts. Individual beds are 15–40 cm thick. In 198VC the shear strength of this facies ranges from 112 to 200 kPa. In 199VC the basal Fmd(c) has a shear strength of 60–65 kPa and a 20-cm-thick bed higher up in the core from 100 to 80 cm depth yielded 45–50 kPa. The average wet bulk density is 2.05 g ml^{-1}, similar to facies Fmd (see below), but the magnetic susceptibility is much higher, averaging 103.7 SI and reaching a maximum 134 SI, probably as a consequence of greater abundance of larger clasts within the muddy matrix (Supplementary Information Figure b). Facies Fmd(c) also contains abundant shell fragments and is particularly rich in foraminifera. In both cores Fmd(c) grades subtly into facies Fld(c). Three samples date the same horizon in Fmd(c) at a depth of 312–314 cm, close the bottom of core 199VC (Fig. 9; Table 2). These comprise ages of 37 229 ± 753 (SUERC-63564), 40 452 ± 631 (SUERC-67942) and 31 915 ± 492 (SUERC-67941) cal a BP from a mixed benthic foraminifera sample, a monospecific *Bulimina elongata* sample and a monospecific *Elphdium clavatum* sample, respectively. A further monospecific *Elphidium clavatum* sample from the base of core 198VC produced an age indistinguishable from background (UCIAMS-186908).

Lithofacies 5. Laminated mud (Fld)

Facies Fld is identified in core 197VC from the Slyne Trough (Fig. 9). It is a dark grey (5Y4/1) laminated, clayey silt that contains dispersed granules and occasional pebbles some of which are draped by overlying laminae. Shell and coral fragments are abundant in this facies. Bioturbation, in the form of burrows, is occasionally present. Lamination style is variable, ranging from sharp and well-defined millimetre to sub-millimetre in thickness to more diffuse. Shear strength of the Fld facies is typically < 25 kPa with a minimum of 9 kPa. Magnetic susceptibility is 1.9 SI and wet bulk density is 92 g ml^{-1} (Supplementary Information Figure b). There are no radiocarbon measurements from this lithofacies.

Lithofacies 6. Massive mud with clasts (Fmd)

Facies Fmd occurs in two cores from the Slyne Trough: 173–55 cm depth in core 198VC and 70–43 cm depth in

Table 1. Location, water depth and recovery of sediment cores discussed in text.

Core name (JC106-)	Location	Water depth (m)	Recovery (m)
158VC	53°48.117′N, 13°7.35′W	295	2.28
159VC	53°47.441′N, 12°59.977′W	316	0.76
161VC	53°44.876′N, 12°59.442′W	267	0.51
167VC	53°39.376′N, 12°46.022′W	257	0.98
168VC	53°39.72′N, 12°42.543′W	246	0.67
169VC	53°41.457′N, 12°41.799′W	277	1.02
170VC	53°41.457′N, 12°41.799′W	267	0.38
172VC	53°47.555′N, 12°46.875′W	271	1.35
176VC	53°38.855′N, 12°17.386′W	292	2.08
177VC	53°36.373′N, 12°4.896′W	277	2.34
180 PC	53°18.322′N, 10°12.677′W	112	6.49
184 PC	53°20.049′N, 10°16.551′W	100	7.90
190VC	53°21.818′N, 11°9.173′W	149	1.97
193VC	53°25.008′N, 11°17.092′W	146	2.58
194VC	53°33.31′N, 11°42.048′W	240	5.24
195VC	53°34.237′N, 11°43.13′W	236	4.18
196VC	53°34.414′N, 11°43.295′W	235	2.38
197VC	53°45.064′N, 11°53.655′W	278	2.44
198VC	53°49.389′N, 11°50.428′W	290	3.85
199VC	53°36.677′N, 12°4.23′W	302	3.29
211VC	53°1.556′N, 11°43.657′W	160	1.94

Table 2. Radiocarbon results for cores discussed in this study.

Publication code	Core	Depth (cm)	Sample type	^{14}C age (a BP) ± 1σ	Calibrated age (cal a BP) ± 2σ $\Delta R = 0$ years	Calibrated age (cal a BP) ± 2σ $\Delta R = 300$ years	Calibrated age (cal a BP) ± 2σ $\Delta R = 700$ years	Bayesian modelled age (ka)	Comment
SUERC-67929	JC106-158VC	160	Shell fragment	Indistinguishable from background					Iceberg turbate – maximum age
SUERC-63578	JC106-158VC	179	Shell fragment	16 414 ± 46	19 328 ± 186	18 949 ± 129	18 586 ± 135		Iceberg turbate – maximum age
SUERC-67930	JC106-158VC	184–185	Shell fragment	15 533 ± 43	18 390 ± 157	18 031 ± 161	17 588 ± 178		Iceberg turbate – maximum age
SUERC-67931	JC106-158VC	184–185	Shell fragment	16 460 ± 44	19 381 ± 174	18 999 ± 139	18 633 ± 122		Iceberg turbate – maximum age
SUERC-63582	JC106-158VC	188–188.5	Shell fragment	14 906 ± 43	17 681 ± 184	17 294 ± 190	16 695 ± 237		Iceberg turbate – maximum age
SUERC-63577	JC106-158VC	58	Shell fragment	25 722 ± 84	29 375 ± 284	29 053 ± 290	28 651 ± 221		Iceberg turbate – maximum age
SUERC-58387	JC106-159VC	68	Shell fragment	Indistinguishable from background					Till – maximum age
SUERC-58389	JC106-167VC	48–49	Shell fragment	21 202 ± 57	25 103 ± 265	24 669 ± 302	24 161 ± 208	24.88 ± 0.23	Till – maximum age
SUERC-67932	JC106-167VC	50–51	Shell fragment	21 452 ± 60	25 398 ± 206	25 023 ± 308	24 431 ± 237	25.16 ± 0.28	Till – maximum age
SUERC-58392	JC106-167VC	61–62	Shell fragment	23 309 ± 66	27 263 ± 192	26 932 ± 312	26 413 ± 263	27.10 ± 0.17	Till – maximum age
SUERC-67933	JC106-167VC	74	Shell fragment	47 431 ± 928					Till – maximum age
SUERC-67937	JC106-167VC	80–81	Shell fragment	21 146 ± 59	25 014 ± 310	24 581 ± 298	24 104 ± 208	24.82 ± 0.18	Till – maximum age
SUERC-58393	JC106-167VC	81–82	Shell fragment	26 895 ± 89	30 786 ± 206	30 533 ± 298	29 997 ± 404	30.54 ± 0.2	Till – maximum age
SUERC-59511	JC106-176VC	69	Coral	29 328 ± 117	33 140 ± 388	32 691 ± 496	32 064 ± 525	32.55 ± 0.19	Till – maximum age
SUERC-59512	JC106-176VC	70.5	Shell fragment	Indistinguishable from background					Till – maximum age
SUERC-59518	JC106-177VC	125	Shell fragment	Indistinguishable from background					Till – maximum age
SUERC-59519	JC106-177VC	132	Shell fragment	Indistinguishable from background					Till – maximum age
SUERC-59520	JC106-177VC	158.5	Shell fragment	24 541 ± 79	28 168 ± 282	27 876 ± 190	27 618 ± 167	27.96 ± 0.2	Till – maximum age
SUERC-60159	JC106-177VC	164–165	Shell fragment	24 529 ± 82	28 155 ± 284	27 868 ± 190	27 611 ± 169	27.95 ± 0.18	Till – maximum age
SUERC-59521	JC106-177VC	168.5	Shell fragment	32 688 ± 171	36 171 ± 390	35 885 ± 402	35 465 ± 447	35.60 ± 0.31	Till – maximum age
SUERC-60160	JC106-177VC	196	Shell fragment	24 365 ± 80	27 986 ± 241	27 754 ± 161	27 515 ± 174	27.82 ± 0.15	Till – maximum age
SUERC-60163	JC106-177VC	214	Shell fragment	Indistinguishable from background					Till – maximum age

(*Continued*)

Table 2. (*Continued*)

Publication code	Core	Depth (cm)	Sample type	^{14}C age (a BP) ± 1σ	Calibrated age (cal a BP) ± 2σ $\Delta R = 0$ years	Calibrated age (cal a BP) ± 2σ $\Delta R = 300$ years	Calibrated age (cal a BP) ± 2σ $\Delta R = 700$ years	Bayesian modelled age (ka)	Comment
SUERC-68872	JC106-177VC	51–52	Whole bivalves, *Yodiella* sp.	15 576 ± 44	18 440 ± 145	18 077 ± 171	17 644 ± 186	18.37 ± 0.09	Iceberg turbate? – maximum age
SUERC-59516	JC106-177VC	83	Shell fragment	35 861 ± 243	40 061 ± 606	39 715 ± 617	39 275 ± 596	39.15 ± 0.43	Till – maximum age
SUERC-59517	JC106-177VC	84	Shell fragment	35 139 ± 225	39 249 ± 564	38 955 ± 527	38 540 ± 508	38.43 ± 0.49	Till – maximum age
SUERC-63562	JC106-180PC	639–640	Mixed benthic foraminifera	14 384 ± 41	16 962 ± 214	16 500 ± 221	15 965 ± 178	16.93 ± 0.16	Glacimarine mud – deglacial (Callard *et al.*, 2020)
UCIAMS-186921	JC106-184PC	763–764	*Yodiella* species	14 471 ± 70	17 101 ± 270	16 640 ± 290	16 076 ± 225		Glacimarine mud – deglacial (Callard *et al.*, 2020)
UCIAMS-186924	JC106-184PC	763–764	*Yodiella* species	14 470 ± 60	17 101 ± 247	16 640 ± 270	16 077 ± 206		Glacimarine mud – deglacial (Callard *et al.*, 2020)
SUERC-68873	JC106-190VC	150–152	Mixed benthic foraminifera	23 316 ± 78	27 267 + 202	26 937 ± 323	26 424 ± 288	27.11 ± 0.17	Deformed glacimarine mud – retreat & readvance (Callard *et al.*, 2020)
UCIAMS-176384	JC106-190VC	180–182	Mixed benthic foraminifera	21 470 ± 90	25 414 + 241	25 029 ± 359	24 478 ± 329	23.06 ± 0.62	Deformed glacimarine mud – retreat & readvance (Callard *et al.*, 2020)
UCIAMS-164434	JC106-190VC	192–194	Mixed benthic foraminifera	19 470 ± 100	22 964 + 329	22 640 ± 251	22 219 ± 267	22.95 ± 0.23	Deformed glacimarine mud – retreat & readvance (Callard *et al.*, 2020)
SUERC-60164	JC106-193VC	251	Shell fragment	22 635 ± 71	26 446 + 284	26 134 ± 206	25 830 ± 155	26.29 ± 0.17	Till – maximum age (Callard *et al.*, 2020)
SUERC-58323	JC106-194VC	514–515	Mixed benthic foraminifera	20 695 ± 53	24 361 + 202	24 050 ± 202	23 603 ± 227	24.19 ± 0.15	Glacimarine mud – deglacial (Callard *et al.*, 2020)
SUERC-60165	JC106-195VC	219–220	Shell fragment	19 387 ± 58	22 849 + 231	22 538 ± 165	22 147 ± 227	24.04 ± 0.41	Glacimarine mud – deglacial (Callard *et al.*, 2020)
SUERC-60167	JC106-195VC	309–310	Shell fragment	52 487 ± 1834					Till – maximum age (Callard *et al.*, 2020)
SUERC-60168	JC106-195VC	314–315	Shell fragment	28 867 ± 126	32 407 + 561	31 982 ± 531	31 485 ± 280		Till – maximum age (Callard *et al.*, 2020)
SUERC-60169	JC106-195VC	377–378	Shell fragment	29 214 ± 125	32 994 + 439	32 485 ± 555	31 903 ± 512		Till – maximum age (Callard *et al.*, 2020)
SUERC-60170	JC106-196VC	145–147	Shell fragment	13 265 ± 45	15 349 + 204	14 879 ± 288	14 046 ± 139		Iceberg turbate – maximum age (Callard *et al.*, 2020)
SUERC-60173	JC106-197VC	150	Shell fragment	28 312 ± 117	31 621 ± 347	31 368 ± 216	31 153 ± 184		Glacimarine mud – maximum age on retreat (reworked sample)
SUERC-60174	JC106-197VC	175	Shell fragment	>51 227					Consolidated glacimarine mud – retreat and readvance
SUERC-63583	JC106-197VC	185–186	Whole valve	30 360 ± 132	34 029 ± 270	33 819 ± 245	33 488 ± 339		Consolidated glacimarine mud – retreat and readvance
SUERC-60175	JC106-197VC	225–226	Shell fragment	24 218 ± 89	27 862 ± 196	27 663 ± 171	27 415 ± 196	27.73 ± 0.12	Till – maximum age

(*Continued*)

Table 2. (*Continued*)

Publication code	Core	Depth (cm)	Sample type	^{14}C age (a BP) ± 1σ	Calibrated age (cal a BP) ± 2σ $\Delta R = 0$ years	Calibrated age (cal a BP) ± 2σ $\Delta R = 300$ years	Calibrated age (cal a BP) ± 2σ $\Delta R = 700$ years	Bayesian modelled age (ka)	Comment
SUERC-60177	JC106-197VC	227–228	Shell fragment	24 438 ± 83	28 061 ± 269	27 802 ± 169	27 559 ± 172	27.88 ± 0.15	Till – maximum age
SUERC-58395	JC106-197VC	Shoe	Gastropod	30 244 ± 126	33 944 ± 247	33 738 ± 243	33 369 ± 363	33.63 ± 0.21	Till – maximum age
SUERC-60178	JC106-197VC	Shoe	Whole valve	23 393 ± 76	27 322 ± 192	27 038 ± 314	26 532 ± 325	27.18 ± 0.18	Till – maximum age
UCIAMS-176385	JC106-198VC	77–80	Foraminifera, monospecific *Elphidium clavata*	18 410 ± 60	21 807 ± 210	21 429 ± 253	20 870 ± 216	21.81 ± 0.11	Glacimarine muds – ice sheet retreat
SUERC-63563	JC106-198VC	243–245	Mixed benthic foraminifera	45 223 ± 723					Glaciamarine debris-flow – ice sheet retreat
UCIAMS-176368	198VC	244–246	Foraminifera, monospecific *Elphidium excavatum*	21 620 ± 90	25 556 ± 237	25 256 ± 282	24 706 ± 355	25.61 ± 0.11	Glaciamarine debris-flow – ice sheet retreat
SUERC-59522	JC106-198VC	327	Shell fragment	Indistinguishable from background					Consolidated glacimarine mud – retreat and readvance
SUERC-59523	JC106-198VC	340	Shell fragment	Indistinguishable from background					Consolidated glacimarine mud – retreat and readvance
UCIAMS-186908	JC106-198VC	378–382	Foraminifera, monospecific *E. excavatum*	Indistinguishable from background					Consolidated glacimarine mud – retreat and readvance
UCIAMS-176386	JC106-199VC	55–57	Foraminifera, monospecific *Elphidium clavata*	19 630 ± 70	23 171 ± 270	22 783 ± 239	22 403 ± 157	23.16 ± 0.14	Glacimarine mud – ice sheet retreat
UCIAMS-176369	JC106-199VC	152–154	Foraminifera, monospecific *E. excavatum*	19 200 ± 70	22 655 ± 221	22 374 ± 171	21 936 ± 241	22.65 ± 0.11	Consolidated glacimarine mud – retreat and readvance
SUERC-59526	JC106-199VC	195	Shell fragment	28 829 ± 115	32 349 ± 539	31 916 ± 500	31 449 ± 247		Consolidated glacimarine mud – retreat and readvance
UCIAMS-186911	JC106-199VC	248–250	Foraminifera, monospecific *E. clavatum*	21 990 ± 130	25 866 ± 221	25 616 ± 280	25 192 ± 404	25.79 ± 0.12	Consolidated glacimarine mud – retreat and readvance
SUERC-58396	JC106-199VC	275	Shell fragment	Indistinguishable from background					Consolidated glacimarine mud – retreat and readvance
SUERC-67941	JC106-199VC	312–314	Foraminifera, monospecific *E. clavatum*	28 531 ± 110	31 915 ± 492	31 533 ± 282	31 264 ± 188	31.51 ± 0.2	Consolidated glacimarine mud – retreat and readvance
SUERC-67942	JC106-199VC	312–314	Foraminifera, monospecific *Bulimina elongata*	36 212 ± 259	40 452 ± 631	40 120 ± 637	39 657 ± 651		Consolidated glacimarine mud – retreat and readvance
SUERC-63564	JC106-199VC	312–314	Mixed benthic foraminifera	33 480 ± 182	37 229 ± 753	36 775 ± 633	36 272 ± 427		Consolidated glacimarine mud – retreat and readvance

(*Continued*)

Table 2. *(Continued)*

Publication code	Core	Depth (cm)	Sample type	^{14}C age (a BP) ± 1σ	Calibrated age (cal a BP) ± 2σ $\Delta R = 0$ years	Calibrated age (cal a BP) ± 2σ $\Delta R = 300$ years	Calibrated age (cal a BP) ± 2σ $\Delta R = 700$ years	Bayesian modelled age (ka)	Comment
SUERC-60158	JC106-211VC	22–23	Shell fragment	17 775 ± 51	20 957 ± 210	20 590 ± 176	20 112 ± 188	20.84 ± 0.11	Iceberg turbate – maximum age (Callard *et al.*, 2020)
SUERC-60179	JC106-211VC	24	Shell fragment	14 627 ± 45	17 319 ± 192	16 871 ± 227	16 287 ± 192		Iceberg turbate – maximum age (Callard *et al.*, 2020)
Beta-334419	CE 10 008–44	180	Coral fragment	20 710 ± 90	24 395 ± 313	24 070 ± 260	23 629 ± 295	24.48 ± 0.19	Till – maximum age (Peters *et al.*, 2015, 2016)
Poz2-66430	CE 10 008–45	94	Single bivalve shell	18 733 ± 197	22 148 ± 438	21 852 ± 512	21 325 ± 530	24.06 ± 0.39	Till – maximum age (Peters *et al.*, 2015, 2016)

199VC (Fig. 9). It is a massive, well-sorted, dark grey (5Y4/1) silt or silty clay with shell and coral fragments. Occasional sandy pods, stringers and black mottles occur, and may represent bioturbation. Bounding contacts are sharp to gradational. The shear strength of this lithofacies ranges from 8 to 35 kPa and averages 15 kPa. The wet bulk density is low, averaging 1.97 g ml^{-1}. The magnetic susceptibility is also low averaging 88 SI (Supplementary Information Figure b). Two monospecific samples of benthic foraminifera *Elphidium clavatum* were collected from close to the top of this facies in both 198VC (77 cm) and 199VC (54 cm). They dated to 21 807 ± 210 (UCIAMS-176385) and 23 171 ± 270 (UCIAMS-176386) cal a BP, respectively (Fig. 9; Table 2).

Lithofacies 7. Clast-supported sandy gravel (Gs)

This facies comprises a clast-supported medium to coarse sandy gravel that contains angular to rounded clasts up to 4 cm in diameter as well as abundant shell and coral fragments (Figs. 8 and 9). Individual beds range from 5 to 65 cm in thickness. The upper contact is either sharp or gradational. Where the contact is gradational, facies Gs fines into graded or massive sand (Sg and Sm facies; see below). Facies Gs is unconsolidated but it has a high average wet bulk density of 2.30 g ml^{-1} and a very high average magnetic susceptibility of 329 SI due to its gravelly nature (Supplementary Information Figures a and b).

Lithofacies 8. Gravelly sand (Sg)

This lithofacies is a massive, unconsolidated, gravelly, medium to coarse sand that contains a high abundance of shell and coral fragments (Fig. 8). It is invariably overlain by massive sand (Sm). Clasts range from gravel to pebble-sized, reaching a maximum of 4 cm, and range from angular to rounded. The sand is olive (5Y4/3) or very dark grey (5Y3/1). Individual beds range from 3 to 50 cm in thickness. The upper contact can be sharp or gradational. Where gradational, Sg fines into facies Sm. This lithofacies is unconsolidated and has a high average wet bulk density and magnetic susceptibility of 217 g ml^{-1} and 296 SI, respectively (Supplementary Information Figure a).

Lithofacies 9. Massive sand (Sm)

The uppermost lithofacies in all the cores consists of a saturated, massive, fine to medium sand that contains frequent shell fragments and occasional pebble and gravel-sized clasts (Figs. 8 and 9). The colour varies from olive (5Y4/3), olive grey (5Y4/2) or dark grey (5Y4/1) and often becomes darker downcore. The upper and lower contacts can be either sharp or gradational. The massive sand is underlain predominantly by gravelly sand (Sg). Individual beds are typically a few tens of centimetres thick. Average wet bulk density and magnetic susceptibility is 1.98 g ml^{-1} and 118.3 SI, respectively, but both values vary between cores and within cores, with high values often correlating with the presence of isolated pebble-sized clasts (Supplementary Information Figures a and b).

Lithofacies associations and interpretations

The nine individual lithofacies identified in cores from the Porcupine Bank are grouped into four lithofacies associations (LFAs) (Figs. 8 and 9). LFA 1: consolidated diamicton association (facies Dmm(c)); LFA2: consolidated mud association (facies Fld(c), Fmd(c)); LFA3: mud-diamicton association (facies Dms, Fld, Fmd); LFA4: sand-gravel association (facies Gs, Sm, sg).

Table 3. TCN sample codes, location, outcrop and lithological information and Bayesian modelled age for samples discussed in text. See Roberts *et al.* (2020) for full sample and site information.

Sample code	Location	Outcrop type	Sample lithology	Bayesian modelled age (ka)
T5BH01	Black Head 53.14528 N, 9.27667 W	Erratic	Granite	13.8 ± 1.1
T5BH02	Black Head 53.14528 N, 9.27883 W	Erratic	Granite	16.99 ± 0.31
T5BH03	Black Head 53.14362 N, 9.27833 W	Erratic	Granite	11.8 ± 1.0
T5CL01	Claddaghuff 53.53500 N, 10.1300 W	Erratic	Granite	16.98 ± 0.29
T5CL02	Claddaghuff 53.5372 N, 10.1304 W	Erratic	Granite	17.0 ± 0.31
T5CL03	Claddaghuff 53.5395 N, 10.1261	Erratic	Granite	17.0 ± 0.30
T5CL04	Claddaghuff 53.5382 N, 10.1270 W	Erratic	Granite	17.0 ± 0.30
T5CL06	Claddaghuff 53.55333 N, 10.1647 W	Erratic	Granite	17.0 ± 0.33
T5CL07	Claddaghuff 53.55467 N, 10.1644 W	Erratic	Granite	16.99 ± 0.31
T5IE01	Illion east 53.48133 N, 9.66740 W	Erratic	Metasandstone	15.53 ± 0.81
T5IE03	Illion east 53.48150 N, 9.66740 W	Erratic	Quartzite	15.81 ± 0.71
T5IM01	Inis Meain 53.06722 N, 9.60805 W	Erratic	Granite	17.0 ± 1.2
T5IM02	Inis Meain 53.07805 N, 9.61278 W	Erratic	Granite	19.09 ± 1.08
T5IM03	Inis Meain 53.07830 N, 9.61260 W	Erratic	Metasandstone	22.3 ± 1.2
T5IM04	Inis Meain 53.07972 N, 9.61028 W	Erratic	Granite	19.72 ± 1.19
T5KK01	Kilkierian 53.31180 N, 9.76940 W	Erratic	Granite	16.99 0.3
T5KK02	Kilkierian 53.31140 N, 9.76970	Bedrock	Granite	17.0 ± 0.3
T5KK03	Kilkierian 53.31100 N, 9.76980	Bedrock	Granite	17.0 ± 0.3
T5KK04	Gowlan East 53.39730 N, 9.68250	Erratic	Granite	16.56 ± 0.3
T5KK05	Gowlan East 53.39760 N, 9.68220	Erratic	Granite	16.54 ± 0.29
T5KK06	Gowlan East 53.39920 N, 9.68320	Erratic	Granite	16.57 ± 0.28
T5MOY01	Moycullen 53.31550 N, 9.18910	Erratic	Granite	16.51 ± 0.32
T5MOY02	Moycullen 53.31518 N, 9.18855 W	Erratic	Granite	16.52 ± 0.32
T5MOY03	Moycullen 53.31572 N, 9.18877	Erratic	Granite	16.54 ± 0.3
T5MOY04	Moycullen 53.31473 N, 9.18915 W	Erratic	Granite	16.56 ± 0.28
T5MOY05	Moycullen 53.31540 N, 9.18890	Erratic	Granite	16.57 ± 0.28
T5OU04	Rossaveel 53.28083 N, 9.51862 W	Erratic	Granite	16.99 ± 0.3
T5OU05	Rossaveel 53.28278 N, 9.51722 W	Erratic	Granite	13.5 ± 1.3
T5OU06	Rossaveel 53.28333 N, 9.51305	Bedrock	Granite	17.03 ± 0.34

LFA 1. Diamicton association (Dmm(c))

Massive matrix-supported diamicton is often the lowermost lithofacies in the cores. It is typically stiff with shear strength values up to 200 kPa. Stratification and grading were not observed. This lithofacies is interpreted as a subglacial till with the high shear strengths consistent with loading and compaction by grounded glacier ice (Evans *et al.*, 2006; Ó Cofaigh *et al.*, 2007, 2013; Evans, 2018). Shell fragments within the diamicton indicate that pre-existing marine sediments were incorporated into the till during glacier overriding, and radiocarbon ages on these reworked shells provide a

Table 4. OSL dates from the study area: sample code, location, age (ka) and Bayesian modelled age (ka). See Roberts *et al.* (2020) for further information on site geomorphology and sedimentology.

Sample code	Location	Age (ka)	Bayesian modelled age (ka)
T5SCAT02	Kilkee SW (Co. Clare) 52.64220 N, 9.73390 W	13.7 ± 3.0	16.99 ± 0.31
T5PYNE02	Pyne's Pit (Co. Clare) 52.68830 N, 9.43170 W	13.3 ± 2.7	16.99 ± 0.31
T5KSW01	Scattery Island (Co. Clare) 52.61020 N, 9.52360 W	14.1 ± 3.6	16.98 ± 0.30
T5TULA01	Tullywee (Co. Galway) 53.56020 N, 9.91850 W	14.8 ± 2.8	15.58 ± 0.97

maximum age for till formation and thus ice sheet advance. The youngest ages are the most instructive in this regard and indicate till formation and the presence of a grounded ice sheet on Porcupine Bank after ~25 cal ka BP. This is also consistent with work by Peters *et al.* (2016) who obtained an age of 24.1 cal ka BP from a reworked shell in till from the bank. Collectively this indicates the presence of a grounded ice sheet on the Porcupine Bank during the LGM and until ~24 cal ka BP.

The matrix-supported diamicton in core 158VC from the north-western Porcupine Bank is also massive and very stiff (average shear strength of 102 kPa and maximum of 125 kPa). This might be consistent with an origin as a subglacial till deposited by grounded ice, but we consider this less likely for the following reasons. First, radiocarbon ages on reworked shells within the diamicton are in the age window of 17.8–19.3 cal ka bp. Callard *et al.* (2020) have recently shown that deglaciation of Porcupine Bank was largely complete by about 23 cal ka BP with the ice sheet grounded on the mid-shelf by this time. This is considerably earlier than the ages on reworked shells in core 158VC and is also consistent with ages of ~22–23 cal ka BP from core site 199VC on the eastern Porcupine Bank. Hence the continued presence of a grounded ice sheet on the outer Porcupine Bank as late as 17.8–19.3 cal ka BP is considered unlikely. Second, seafloor bathymetric data from the site of 158VC show that the surface of the GZW from which this core was collected is covered in an extensive series of elongate furrows consistent with iceberg scours (Fig. 5D). We therefore suggest that the massive, matrix-supported muddy diamicton in 158VC is probably a product of formation in a glacimarine environment in which grounded iceberg keels intermittently scoured the seafloor and consolidated the sediment (cf. Dowdeswell *et al.*, 1994; Sacchetti *et al.*, 2012). The date of 18.4 cal ka BP on the articulated bivalve of *Yodiella* species from close to the top of the diamicton in core 177VC is also anomalously young. It may represent incorporation of younger material into the top of the till through localized reworking, e.g. by mass flow or bottom current activity.

LFA2. Consolidated mud association (facies Fld(c), Fmd(c))

This lithofacies association comprises laminated and massive muds with clasts. In many respects these sediments are similar to LFA3 (notably facies Fld and Fmd) but are characterized by higher shear strengths of up to 200 kPa. Furthermore, in some cores (e.g. 197VC) facies Fld(c) laminations are contorted and/or interbedded with deformed silts. Laminated and massive muds with clasts are characteristic of deposition by a range of subaqueous processes in glacimarine and glacilacustrine environments by suspension settling through the water column, iceberg rafting and sediment gravity flows (cf. Powell, 2003). A glacimarine environment is consistent with the presence of abundant *E. clavatum*, a benthic foraminifer that tolerates low-salinity, cold water environments. However, the highly consolidated nature of the matrix of facies Fld(c) and Fmd(c) is difficult to reconcile with *in situ* glacimarine sediments. Rather, it points to a two-stage depositional process in which initial subaqueous deposition of laminated and massive glacimarine muds was followed by ice-marginal overriding and glacitectonic compaction (cf. Ó Cofaigh *et al.*, 2011). Hence the sediments of LFA2 are regarded here as glacitectonites (*sensu* Benn and Evans, 1996; Evans *et al.*, 2006; Evans, 2018). This implies a period of ice-free conditions before ice-sheet readvance and overriding (cf. Peters *et al.*, 2015, 2016).

Radiocarbon measurements from LFA2 were obtained on a mix of samples, comprising individual shell fragments, monospecific samples of benthic foraminifera and mixed benthic foraminiferal samples. All of these ages provide maximum age estimates for the overriding and glacitectonism. The youngest, a monospecific *E. clavatum* sample from core 199VC dated at 22 655 ± 221 cal a BP indicates the core site was ice-free at this time but was subsequently overridden. A second sample of monospecific *E. clavatum* from 248 cm depth in the core dated at 25 866 ± 221 cal a BP also indicates ice-free conditions and a glacimarine sedimentary environment at this time and before overriding (Fig. 9; Table 2). However, most of the samples are considerably older. Indeed, monospecific samples of *E. clavatum* from the base or close to the base of cores 198VC and 199VC gave a non-finite age and an age of 31 915 ± 492 cal a BP, respectively (Fig. 9; Table 2). The latter age on *E. clavatum* was obtained on a sample from 312 to 314 cm depth where we also dated a mixed benthic foram sample (37 229 ± 753 cal a BP) and a monospecific sample of the warm water species *Bulimina elongata* (40 452 ± 631 cal a BP). This was done to assess the impact of a mix of warm and cold species on the age of the mixed sample. The monospecific *E. clavatum* age is the youngest of the three and implies the presence of glacimarine conditions on the bank at ~32 cal ka BP, before ice advance and overriding.

LFA3. Mud-diamicton association (facies Dms, Fld, Fmd)

Collectively this LFA is interpreted as recording deglacial glacimarine sedimentation associated with retreat of grounded ice on Porcupine Bank. Stratified, matrix-supported diamicton is interpreted as the product of subaqueous cohesive debris flow deposition based on the inclined stratification, textural banding and interbedding of poorly sorted diamictons with more silty horizons (Postma, 1986; Eyles and Eyles, 2000; Mulder and Alexander, 2001; Talling *et al.*, 2012). The change in facies upcore from consolidated laminated muds (Fld(c)) interpreted as glacitectonites (see above) into stratified debris flow diamictons with low shear strengths (Dms) in core 198VC is consistent with a change in depositional environment from

subglacial to deglacial associated with the retreat of grounded ice. A monospecific sample of *E. clavatum* from 2 cm above this contact is dated at 25 556 ± 237 cal a BP (Fig. 9) and provides the best constraint on the timing of final ice-sheet retreat from the outer Porcupine Bank.

Laminated mud with dispersed clasts (facies Fld) is inferred to be a product of meltwater sedimentation in which mud emplacement was by suspension settling from turbid meltwater plumes issuing from the retreating grounding-line during deglaciation and supplemented by fine-grained turbidity currents (cf. Mackiewicz *et al.*, 1984; Hesse *et al.*, 1997; Ó Cofaigh and Dowdeswell, 2001; Lucchi *et al.*, 2013). The presence of clasts draped by overlying laminae supports an interpretation of suspension settling through the water-column of fine-grained sediment interspersed with the episodic delivery of coarser ice-rafted debris (Thomas and Connell, 1985).

Massive mud with clasts (facies Fmd) is also interpreted as a product of rapid suspension settling of fine-grained material from meltwater plumes combined with iceberg rafting (Domack, 1984; Dowdeswell *et al.*, 1994). The presence of well-preserved *E. clavatum* indicates that this occurred in a glacimarine setting. The production of such massive glacimarine muds may reflect changes in the position of the grounding-line with the massive structure signifying a more distal setting. Alternatively, it could signify a more proximal location where rapid sedimentation acted to suppress laminae formation. Radiocarbon ages from monospecific samples of *E. clavatum* (see above) indicate the presence of glacimarine conditions, and thus recession of grounded ice, by ~23 cal ka BP.

LFA4. Sand-gravel association (facies Gs, Sm, Sg)

These facies form the uppermost LFA in the sediment cores (Figs. 8 and 9). They comprise a series of variably sorted sand and gravelly facies that are massive and contain abundant shell and coral fragments. Such facies have been commonly described from the uppermost part of the Quaternary sediment sequence on the Atlantic shelf along the Irish margin (Peters *et al.*, 2015, 2016; Callard *et al.*, 2018; Ó Cofaigh *et al.*, 2019) and we interpret them similarly as postglacial in origin, formed predominantly by bottom current activity on the shelf (cf. Howe *et al.*, 2001). Dating constraints on this LFA, however, are poor. The lower boundary of LFA4 is typically erosional and the closest ages to it are from the top of the underlying muds of LFA2 and LFA3. These provide a range of ages of ~ 21–23 cal ka BP on monospecific samples of benthic foraminifera (*E. clavatum*). We therefore infer the presence of a hiatus due to bottom current erosion associated with formation of LFA4. We do not consider LFA4 further in this paper.

Advance and retreat of the last BIIS across Porcupine Bank

GZWs and moraine ridges combined with dated subglacial tills in sediment cores from across the northern Porcupine Bank indicate an extensive BIIS, which reached the outer shelf during the gLGM. Radiocarbon dates on reworked shells within subglacial tills and glacitectonites provided a range of ages from non-finite to finite. Ages on these shells constrain the timing of open-marine conditions on the shelf, as the marine fauna must have originally lived in open water. However, they also provide a maximum age for the enclosing subglacial deposits and therefore ice sheet advance during which the marine fauna and their host sediments were cannibalized and reworked subglacially. Such glacially reworked shell populations typically contain a mixture of ages, and in these cases it is the age of the youngest shells that constrain the timing of till formation and ice sheet advance (Ó Cofaigh *et al.*, 2007; England *et al.*, 2009; Callard *et al.*, 2018). Several cores (167VC, 177VC, 197VC) contain reworked shells in overconsolidated subglacial sediments which yielded ages in the range of ~28.1–25.1 cal ka BP (Figs. 8 and 9; Table 2), indicating advance of grounded ice across Porcupine Bank after ~25.1 cal ka BP and thus during the gLGM. A gLGM age for grounded ice on Porcupine Bank is also indicated by an age of ~24.1 cal ka BP which provides a maximum age constraint on subglacial till in core CE 10008-44 (Peters *et al.*, 2016), implying that grounded ice was still present on the bank at ~24 cal ka BP.

Radiocarbon ages on monospecific samples of benthic foraminifera (*E. clavatum*) from glacimarine sediments constrain the timing of the retreat of grounded ice from outer Porcupine Bank. The key age in this regard is from core 198VC where the vertical transition from glacitectonized, consolidated glacimarine muds (facies Fld(c), indicating the presence of grounded ice) into the overlying stratified diamicton formed by subaqueous debris flow during deglaciation produced an age of 25 556 ± 237 cal a BP (see above). There is no evidence that the debris-flow diamicton was subsequently overridden by grounded ice and so this age constrains the timing of final retreat from outer Porcupine Bank. It overlaps with an age of 25 886 ± 221 cal a BP obtained on a further monospecific sample of well-preserved *E. clavatum* from overridden glacimarine muds in core 199VC, located 27 km inshore of 198VC. The sequence in 199VC implies that, following initial grounding-line retreat and glacimarine sedimentation, the ice sheet readvanced over the glacimarine sediments at this core site and deformed them. Hence the latter age provides both a maximum age for this readvance and a minimum age for initial retreat. Collectively these two ages indicate that ice retreat from outer Porcupine Bank was underway before 25.5–25.8 cal ka BP. Deglaciation of the BIIS from Porcupine Bank, the westernmost extent achieved by the ice sheet, therefore commenced relatively early during the gLGM and c. 3–4 ka earlier than previous reconstructions have suggested (Peters *et al.*, 2016).

Sedimentological and radiocarbon data indicate that ice sheet retreat from the Porcupine Bank was not a continuous process but was interrupted by stillstands of the grounding line and readvances of up to a few kilometres. This is indicated by the presence of overridden glacimarine sediments in several cores (197VC, 198VC, 199VC) as well as early ages of ~25.5–25.8 cal ka BP for initial retreat, combined with younger ages of ~24.1–25.1 cal ka BP for subglacial tills and glacitectonites (e.g. cores 167VC and CE10008-44). The often well-preserved lamination within these overconsolidated glacitectonites implies relatively short transport distances and relatively low strain rates, possibly close to the grounding-line, where complete homogenization of the glacimarine sediments did not occur (cf. Ó Cofaigh *et al.*, 2011; Evans, 2018). The occurrence of readvances during ice-sheet retreat from the Porcupine Bank is also supported by the work of Callard *et al.* (2020) who reported a deglacial age of ~24.4 cal ka BP from laminated glacimarine muds at the base of core 194VC in the Slyne Trough, indicating that the grounding-line was located inshore of this core site by that time. However, in the upper part of the core the laminated sediments are glacitectonized, indicating they were subsequently overridden. Furthermore, the sequence of GZWs and moraines across the outer Porcupine Bank (Figs. 4-7) is consistent with an oscillating grounding-line which underwent periodic readvance over deglacial glacimarine sediments (cf. Peters *et al.*, 2015, 2016).

Glacitectonized deglacial subaqueous facies are characteristic of many areas of the last BIIS where it underwent retreat in a marginal glacimarine or glacilacustrine environment (e.g. Hambrey *et al.*, 2001; Ó Cofaigh and Evans, 2001; Evans and Ó Cofaigh, 2003; Roberts and Hart, 2005; Hiemstra *et al.*, 2006; Chiverrell *et al.*, 2018; Roberts *et al.*, 2018; Ó Cofaigh *et al.*, 2011, 2012b, 2019; Callard *et al.*, 2018, 2020).

Grounding-line retreat occurred in a glacimarine environment. Peters *et al.* (2016) first proposed that this was as an ice shelf rather than a tidewater margin. The presence of GZWs within deeper water, notably within the Slyne Trough, suggests that vertical accommodation space in front of the grounding-line was limited and is consistent with formation in an ice-shelf cavity (Dowdeswell and Fugelli, 2012). However, the sharp-crested moraines in shallower water across Porcupine Bank (Fig. 6) are more indicative of a grounded tidewater ice margin (see Batchelor and Dowdeswell, 2015 and references therein). We suggest that the nature and distribution of the deglacial landforms across the Porcupine Bank and Slyne Trough record local variability in accommodation space along the BIIS grounding-line during retreat, as reflected in lateral transitions from a grounded tidewater front to an ice shelf. In terms of lithofacies, sediments deposited at ice-shelf grounding lines are characterized by coarse-grained facies, often represented as stratified diamictons which transition upwards into laminated and massive muds (e.g. Kilfeather *et al.*, 2011; Smith *et al.*, 2019). Core 198VC from the outer Slyne Trough preserves a sequence of subglacial sediments overlain by deglacial stratified diamicton and massive mud. It is possible therefore that this reflects sedimentation with increasing distance from the grounding-line in an ice shelf cavity. However, it is equally plausible that this sequence and the massive-laminated glacimarine muds found in other cores from the Slyne Trough represent tidewater glacimarine sediments produced by ice-marginal debris flows, suspension-settling and rain-out of ice-rafted debris (Mackiewicz *et al.*, 1984; Powell and Domack, 1995). Thus, although there is geomorphological support for ice-shelf development within the Slyne Trough during deglaciation, the sedimentological data are more equivocal.

Bayesian analysis and palaeoglaciological reconstruction

We now use a Bayesian temporal model to reconstruct the pattern of ice sheet retreat from the outer shelf offshore of western Ireland to a few tens of kilometres inshore of the present coastline (Figs. 11 and 12). For full details of the Bayesian model see the Methods section. We divide our reconstruction into three geographical areas: (1) Porcupine Bank and the Slyne Trough, (2) the mid- to inner shelf, including the Aran Islands, and (3) inland from the present coastline. We thus capture the 'marine to terrestrial transition'.

Porcupine Bank and the Slyne Trough

Across the northern Porcupine Bank, GZWs and moraines, combined with subglacial tills and glacitectonites, provide evidence for a grounded ice sheet that extended to the outer shelf during the gLGM. The Bayesian analysis indicates that the maximum position was attained by 26.8 ± 1.33 ka BP (Boundary Layer 1, Fig. 12), and that retreat was underway by 25.9 ± 1.8 ka BP (Boundary Layer 2, Fig. 12). The presence of well-preserved glacimarine benthic foraminifera in deglacial lithofacies implies that retreat took place in a glacimarine environment, and that glacimarine conditions prevailed across the bank until 25.4 ± 0.25 ka BP (Boundary Layer 3, Fig. 12). Ages on reworked shells from tills and overridden glacimarine sediments on the outer shelf indicate that the ice sheet readvanced onto the bank, and probably oscillated there, until c. 24.3 ± 0.19 ka BP (Boundary Layer 4, Fig. 12) when it underwent retreat towards the mid-shelf (Fig. 12). The geomorphology, sedimentology and radiocarbon chronology are therefore consistent with an extensive ice sheet that was grounded on the outer shelf at the gLGM (cf. Peters *et al.*, 2015, 2016), which commenced retreat also during the gLGM, but then oscillated during deglaciation. Such early BIIS retreat is consistent with recent work from further to the north in Donegal Bay (Ó Cofaigh *et al.*, 2019) and the Malin Sea shelf (Callard *et al.*, 2018), and also from the Celtic Sea sector to the south (Scourse *et al.*, 2019).

Mid-inner shelf

Sub-bottom profiler data from across the mid- to inner shelf reveal a series of well-developed GZWs and intervening smaller moraines indicating episodic retreat across the shelf (Callard *et al.*, 2020). The largest of these GZWs has been referred to variously as the 'Mid-Shelf Grounding-Zone Complex' (Callard *et al.*, 2020) or 'Galway Lobe Grounding-Zone Wedge' (Peters *et al.*, 2016). It is a composite, multi-crested feature containing over-ridden glacimarine muds and formed at an oscillating grounding line which glacitectonized deglacial subaqueous sediments. Across the mid-shelf, individual GZWs are separated by sedimentary basin fills, and cores from these basins recovered overridden glacimarine sediments. Callard *et al.* (2020) interpreted the basin fills as having formed by a two-stage depositional process in which initial glacimarine sedimentation took place in front of the grounding line when the ice sheet was positioned at a GZW, followed by grounding-line readvance(s) which overrode and deformed the deglacial sediments (cf. Peters *et al.*, 2016).

The BIIS grounding-line had retreated to the Mid-Shelf Grounding-Zone Complex and was oscillating in this position by 23.7 ± 0.45 ka BP (Boundary Layer 5, Fig. 12). Hence the Porcupine Bank and Slyne Trough were ice-free by this time. Retreat from the Mid-Shelf Grounding-Zone Complex back to the Aran Islands on the inner shelf had occurred by c. 22.0 ± 1.12 ka BP (Boundary Layer 6, Fig. 12). Grounding-line retreat at this time is consistent with glacimarine sedimentation in the Slyne Trough dated to ~22.8 cal ka BP (Callard *et al.*, 2020). A minimum age for the timing of deglaciation of the inner shelf is provided by an age of 17.1 cal ka BP in glacimarine sediments (Callard *et al.*, 2020). However, the Bayesian modelling of TCN ages obtained for glacially transported, erratic boulders of Galway granite resting on Carboniferous limestone bedrock on Inish Mean, the middle of the three Aran Islands (see Roberts *et al.*, 2020), suggests that these sites were ice-free by 19.5 ± 0.8 ka BP (Fig. 12; Table 3).

Terrestrial transition

TCN ages primarily obtained from glacially transported, erratic boulders constrain the timing of ice sheet retreat onto mainland Ireland and then further inland into the mountains of Connemara (Roberts *et al.*, 2020) (Table 3). These ages in the Bayesian analysis indicate that the ice sheet had retreated from the inner shelf onto mainland Ireland by 17.3 ± 0.46 ka BP (Boundary Layer 7, Fig. 12) and imply a relatively slow retreat from the Aran Islands (deglaciated by 19.5 ± 0.8 ka BP) back onto the coastline. The Aran Islands may have acted as a pinning point on the inner shelf, stabilizing the BIIS grounding-line and thus slowing overall ice sheet retreat.

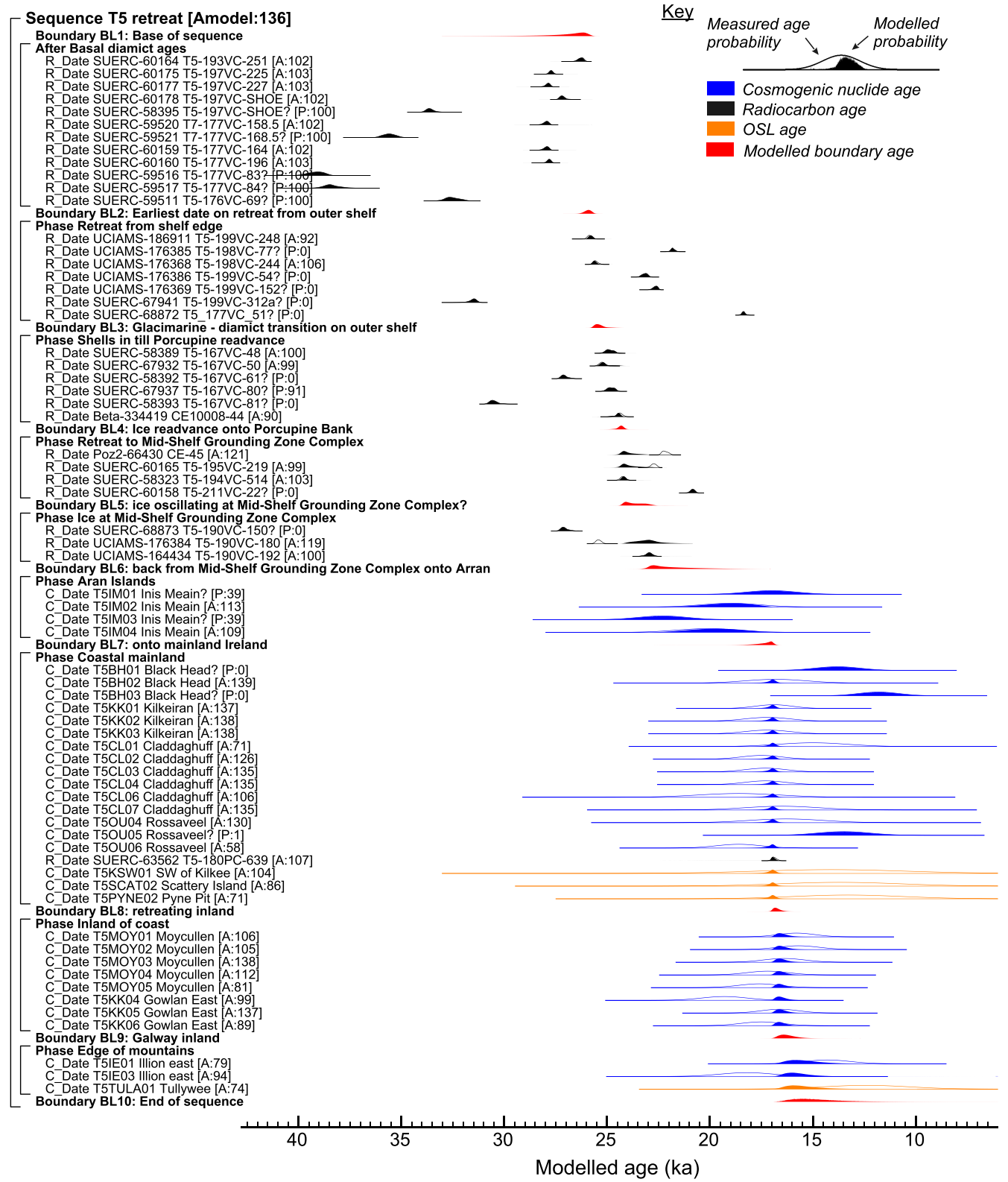

Figure 11. Bayesian age-model output for age measurements constraining the timing of ice sheet retreat in western Ireland and the adjoining continental shelf using OxCal (Bronk Ramsey, 2009). Agreement index (A-values in square brackets) shown alongside chronosequence conformability. P-values < 20 (in square brackets) denote outliers (underlined). Modelled age in ka cal BP on the *x*-axis. Each distribution (light grey) represents the relative probability of each age estimate with posterior density estimate (colour) generated by the modelling. Shown are ^{14}C ages (green), TCN ages (blue), OSL ages (orange) and modelled boundary ages (black). Each distribution represents the relative probability of each age estimate with posterior density estimate (coloured) generated by the modelling. [Color figure can be viewed at wileyonlinelibrary.com]

TCN ages on erratic boulders along the Connemara coastline or from a few kilometres inland constrain the timing of ice sheet retreat inland from the coast (see Roberts *et al.*, 2020). This phase of retreat was underway by 16.8 ± 0.2 ka BP (Boundary Layer 8, Fig. 12). At this time the BIIS grounding-line had stepped back from the inner shelf and the ice sheet was largely terrestrially based, although it is possible that, locally, parts of the ice sheet were marine-terminating and still calving icebergs onto the inner shelf. TCN ages on glacial erratics from sites further inland (Roberts *et al.*, 2020) constrain the timing of subsequent north-eastward ice sheet recession inland to the foothills of the mountains. The Bayesian analysis

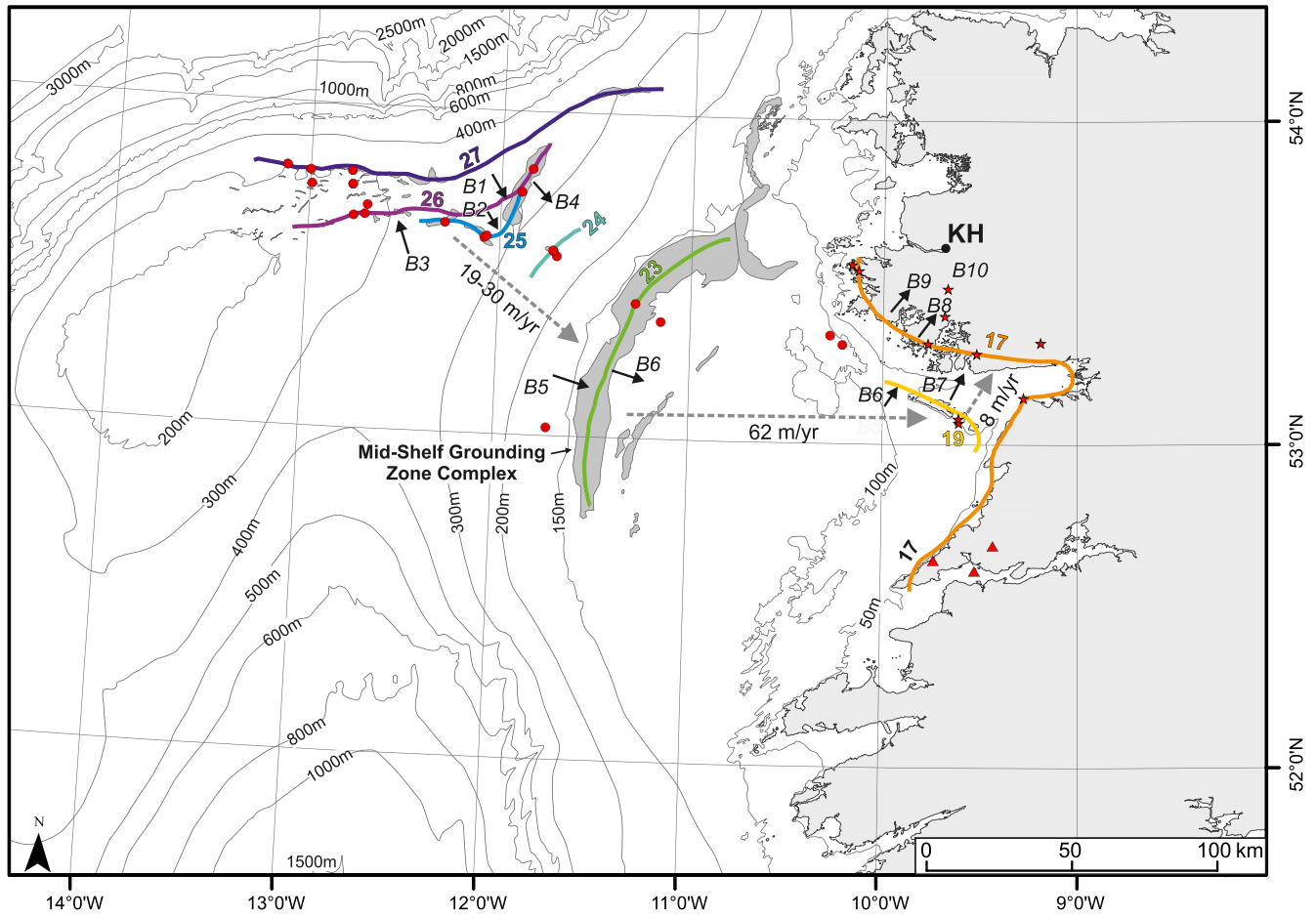

Figure 12. Maximum and retreat grounding-line positions of the British–Irish Ice Sheet on the continental shelf offshore western Ireland and across the present-day coastal hinterland. Location of the geochronological sites constraining the Bayesian modelling, modelled ages for retreat positions, major glacial landforms on the shelf (moraines and grounding-zone wedges) and isochrones are shown. B1-10 = Boundary Layers 1–10, KH = Killary Harbour. Bathymetric data are from INFOMAR (Integrated Mapping for the Sustainable Development of Ireland's Marine Resource; Geological Survey of Ireland and Marine Institute). **B1** (**Boundary Layer 1**) – base of sequence 26.8 ± 1.33. **B2 (Boundary Layer 2)** – earliest date on retreat from outer shelf 25.9 ± 1.8. **B3 (Boundary Layer 3)** – end of ice-free conditions before readvance onto Porcupine Bank 25.4 ± 0.25. **B4 (Boundary Layer 4)** – onset of retreat following readvance onto Porcupine Bank 24.3 ± 0.19. **B5 (Boundary Layer 5)** – ice oscillating at the 'Mid-Shelf Grounding Zone Complex' 23.7 ± 0.45. **B6 (Boundary Layer 6)** – retreat from the 'Mid-Shelf Grounding Zone Complex' onto Aran 22.0 ± 1.12. **B7 (Boundary Layer 7)** – retreat onto mainland Ireland 17.3 ± 0.46. **B8 (Boundary Layer 8)** – retreat inland 16.8 ± 0.2. **B9 (Boundary Layer 9)** – retreat inland 16.3 ± 0.42. **B10 (Boundary Layer 10)** – end of sequence 15.0 ± 1.35. [Color figure can be viewed at wileyonlinelibrary.com]

places this phase of retreat at 16.3 ± 0.42 ka BP (Boundary Layer 9, Fig. 12) and the ice sheet had receded back to the foothills by 15.0 ± 1.35 ka BP (Boundary Layer 10, Fig. 12). We infer that at this time the ice sheet was predominantly terrestrially based, and this is supported by reconstructions of RSL in this area, which indicate that RSL remained below present between 20 and 10 ka BP (Edwards and Craven, 2017; Roberts *et al.*, 2020). Interestingly, however, Callard *et al.* (2020) suggested that the ice sheet may locally have had a marine-terminating margin on the shelf as late as ~15.6 ka BP based on dated evidence of iceberg turbation on the mid-shelf slope. This is also consistent with Peters *et al.* (2016) who proposed that their 'Connemara Lobe', an outlet glacier emanating from Killary Harbour (Fig. 12), overrode marine sediments dating to c. 15.1 cal ka BP.

Discussion

Extent of the BIIS on the Atlantic shelf west of Ireland during the LGM

Early terrestrially-based models of the extent of the last BIIS in western Ireland can be divided into two broad hypotheses (Ballantyne *et al.*, 2008; Ballantyne and Ó Cofaigh, 2017): (1) at the LGM the ice sheet limit was located onshore at a moraine belt termed the Ballycastle–Mulrany limit leaving ice-free terrain beyond this limit, both north and south of Clew Bay (e.g. Charlesworth, 1928; Orme, 1967; Synge, 1968, 1979; Bowen et al, 2002; Knight *et al.*, 2004); and (2) at the LGM the ice sheet extended offshore onto the adjoining continental shelf (e.g. Hallissy, 1914; Warren, 1991, 1992). As noted by Ballantyne *et al.* (2008), however, both hypotheses contain uncertainties. These mainly centred on, firstly, the age of the 'unglaciated' terrain beyond the LGM limit as to whether this was 'Munsterian' (Knight *et al.*, 2004) or Early Midlandian in age (Bowen *et al.*, 2002; McCabe *et al.*, 2007), and, secondly, whether the mountains of Connemara represented a barrier to ice flowing west from the Irish Midlands or acted as an independent centre of ice dispersal.

Ballantyne *et al.* (2007, 2008) used trimline evidence and TCN dating to constrain the altitude and deglaciation chronology of the last ice sheet in western Ireland. Although the trimlines were initially interpreted as marking the upper limit of the ice sheet, subsequent research showed that they represent an englacial transition between warm-based erosive ice on lower ground and cold-based ice over higher ground and summits (Ballantyne *et al.*, 2011; Ballantyne and

Stone, 2015), implying that the trimlines record the minimum, rather than maximum, altitude of the LGM ice surface. It is likely that the last ice sheet overtopped all the Connemara mountains, which appear to have acted as an independent centre of ice dispersal throughout the lifetime of the last ice sheet, diverting ice from the Irish Midlands both north-west into Clew Bay and south-west into Galway Bay (Ballantyne and Ó Cofaigh, 2017).

The earliest direct evidence supporting the presence of grounded ice on the Atlantic shelf west of Ireland was reported by King *et al.* (1998) who used reflection seismic data to document a series of north–south-orientated moraines. They proposed that the outermost moraine positioned at the shelf edge, although not dated, represented the LGM limit (Sejrup *et al.*, 2005). Subsequent glacial geomorphological mapping from the Malin Sea and offshore of Donegal Bay (Fig. 1) using the Olex bathymetric database and high-resolution multibeam swath bathymetry data provided compelling evidence for the presence of grounded ice in the form of drumlins and nested arcuate moraines (Benetti *et al.*, 2010; Dunlop *et al.*, 2010, 2011; Ó Cofaigh *et al.*, 2012a). A shelf-edge-terminating ice sheet during the LGM offshore of northwest Ireland and western Scotland was subsequently confirmed by the evidence provided by dated sediment cores, which indicated that the ice sheet was grounded at the Malin Shelf edge at ~26.5–26.2 cal ka BP (Callard *et al.*, 2018; Ó Cofaigh *et al.*, 2019). Farther south on the shelf offshore of Galway Bay, ^{14}C dates obtained for marine fauna in sediment cores from the Porcupine Bank by Peters *et al.* (2015, 2016) suggested that grounded ice advanced onto the bank after ~24.1 cal ka BP and did not commence retreat until ~21.8 cal ka BP.

The data presented here support these earlier findings and conclusively demonstrate BIIS advance to the outer Atlantic shelf offshore of western Ireland early in the gLGM (Fig. 12). This finding is consistent with a step-wise increase after 26.5 ka BP in the flux of ice-rafted debris to core site MD01-2461, located on the north-western flank of the Porcupine Seabight (Figs. 1 and 2) (Peck *et al.*, 2007). A consistent picture therefore emerges of an extensive BIIS offshore of west and north-west Ireland during the gLGM (Ó Cofaigh *et al.*, 2012a, 2019; Peters *et al.*, 2015, 2016; Callard *et al.*, 2018, 2020; this study). This revises previous interpretations that the LGM ice sheet was not as extensive as that of Marine Isotope Stage 3 (MIS3) (cf. Bowen *et al.*, 2002; McCabe *et al.*, 2007), or terminated at the Mid-Shelf Grounding-Zone Complex (cf. Clark *et al.*, 2012; McCarron *et al.*, 2018). The evidence presented here suggests that the LGM advance was probably at least as extensive as any preceding earlier advance(s) across the western shelf.

The Bayesian analysis indicates that ice sheet retreat from outer Porcupine Bank was underway by 25.9 ka BP (Fig. 12). This indicates a relatively short period (< 1000 years) of ice sheet grounding at its maximum position on the outer shelf before retreat commenced. Thus, the maximum position may not have been a steady-state ice sheet configuration. However, retreat from Porcupine Bank was not a continuous process. It was punctuated by a series of readvances of up to a few kilometres in extent, as indicated by dated, overridden glacimarine sediments and tills, as well as GZWs and moraines. These provide compelling evidence for an ice sheet that was intermittently grounded on Porcupine Bank as late as c. 24.3 ka BP based on the Bayesian analysis (cf. Peters *et al.*, 2016; Callard *et al.*, 2020; this study). This implies that although the ice sheet underwent early initial retreat and was characterized by oscillatory behaviour during deglaciation, it maintained an outer shelf position for c. 1500 years. However, deglacial sediments dated to 25.5 ka BP in core 198VC are not subsequently overridden; hence, any such readvances/oscillations did not reach the shelf edge.

Timing and controls on ice sheet retreat

Retreat of the last BIIS from the outer shelf west of Ireland was underway by 25.9 ka BP and thus early during the gLGM (Fig. 12). Early deglaciation of the Porcupine Bank is consistent with recent studies from the continental shelf offshore of northwest Ireland and Scotland, where retreat was underway by 25–26 ka BP (Callard *et al.*, 2018; Ó Cofaigh *et al.*, 2019). It is also consistent with the retreat of the Irish Sea Ice Stream from the shelf edge of the Celtic Sea at c. 25 ka BP (Scourse *et al.*, 2019). Initial deglaciation of the BIIS from the Atlantic shelf west of Ireland and in the Celtic Sea was therefore largely synchronous. Retreat west of Ireland commenced during Greenland Stadial 3 (GS-3, 27.5–23.3 ka; Rasmussen *et al.*, 2014), and this period also encompasses final retreat of the grounding-line off Porcupine Bank and back towards the Mid-Shelf Grounding Zone Complex at c. 24.3 ka BP (Fig. 13C). We therefore rule out atmospheric warming as the trigger for initial deglaciation of the bank.

A recent study of deglacial benthic foraminiferal populations from the Porcupine Bank and western Irish shelf indicates the persistence of glacimarine conditions until c. 20.9 cal ka BP on the outer shelf, and at least c. 18.5 cal ka BP on the mid-shelf (Peters *et al.*, 2020). Several deep-water cores from along the Irish margin, notably core OMEX-2K from the Goban Spur (Scourse *et al.*, 2009; Haapaniemi *et al.*, 2010) and core MD01-2461 from the Porcupine Saddle (Peck *et al.*, 2007), contain high percentages of *N. pachyderma sinistral* during this period, implying low sea-surface temperatures (Fig. 13D). The absence of a clear ocean warming signal suggests that initial retreat was not triggered by ocean forcing.

Rather, we propose that initial deglaciation and retreat across the Porcupine Bank was driven, at least in part, by high RSL. Current water depths in the outer Slyne Trough are 290–340 m. Assuming eustatic sea level was c. 134 m lower than present early in the gLGM (Lambeck *et al.*, 2014), water depths in the Slyne Trough would still have been in the range of c. 156–206 m. Indeed, this would have been a minimum estimate, as it does not take into account the effects of glacioisostatic depression of the outer shelf related to the presence of an extensive grounded Irish Ice Sheet at glacial maximum. Glacioisostatic adjustment modelling indicates water depths of ~203 m in the central Slyne Trough at 25–26 ka BP (Fig. 13E). High RSL is thus a plausible explanation for triggering initial pull-back and retreat across the bank (cf. Eyles and McCabe, 1989; Ó Cofaigh *et al.*, 2019; Scourse *et al.*, 2019). The inference of high RSL and low water temperatures is supported by the presence of benthic glacimarine foraminifera and associated lithofacies in sediment cores from the Slyne Trough (see 'Sedimentology and radiocarbon measurements' above; cf. Peters *et al.*, 2020).

The Bayesian analysis indicates that the gLGM ice-sheet offshore of western Ireland had a duration of < 1000 years on the outer shelf. It also implies that retreat from the bank was interrupted by a series of readvances/oscillations as recorded by back-stepping GZWs, moraines and overridden glacimarine sediments (Figs. 3–9). The ice sheet had retreated to, and was oscillating at, the Mid-Shelf Grounding Zone Complex by 23.7 ka BP (Fig. 12). This feature marks a major grounding-line position as implied by its large size (> 20 km wide), composite, multi-crested form and internal structure which contains overridden glacimarine sediments. Seismic records from the grounding-zone complex indicate that it forms the upper part of over 70 m of Quaternary sediments and that it most likely represents formation during multiple glacial cycles (McCarron *et al.*, 2018). Stabilization at this position during the last deglaciation may have been facilitated by the bathymetric

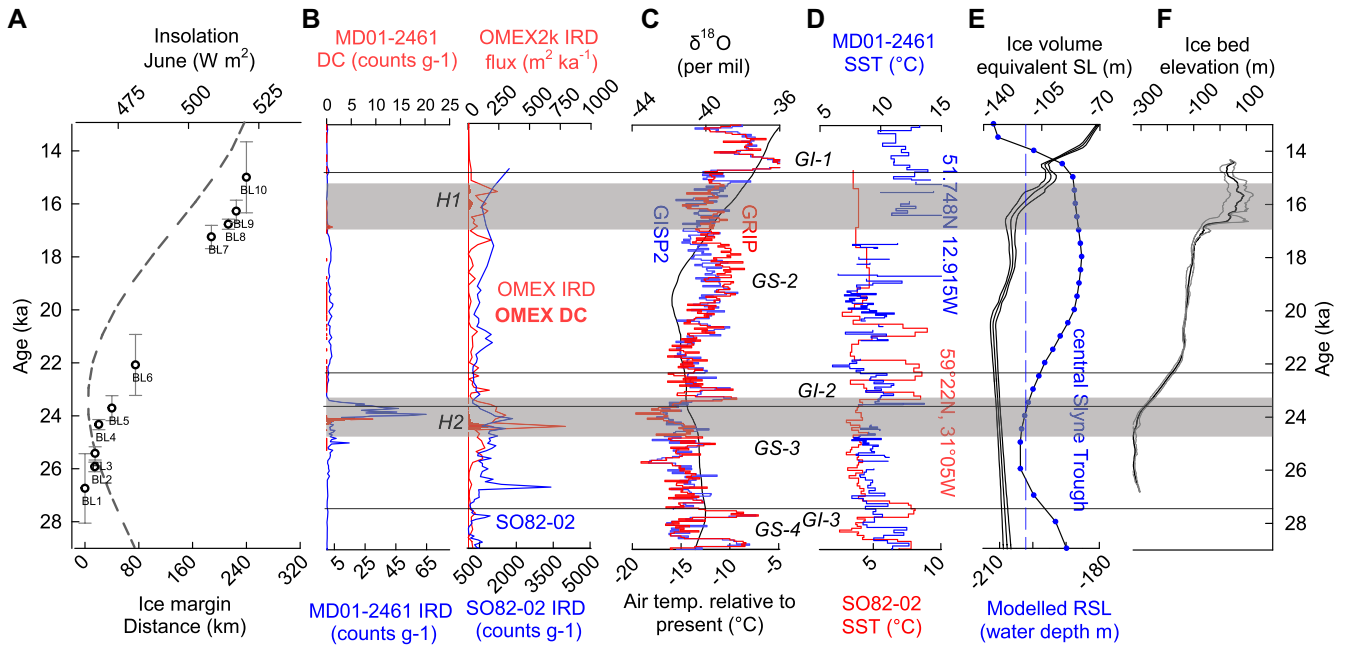

Figure 13. Proxy records of potential deglacial forcing for the last BIIS offshore of western Ireland. (A) The boundary ages (circle ± 1 sigma whisker plots) from the Bayesian model plotted against net axial retreat distance and summer insolation data for 60°N (Berger and Loutre, 1991). (B-left) The dolomitic carbon (DC – solid orange) and total ice-rafted debris (IRD – grey outline) flux records from core MD01-2461 on the Porcupine Seabight at 51.7°N, 12.9°W (left) (Peck *et al.*, 2006, 2007) and (B-right) and core OMEX2K from the Goban Spur continental slope south-west of Ireland (Haapaniemi *et al.*, 2010), alongside total IRD from North Atlantic core SO82-2 from the Reykjanes Ridge at 59°N (Moros *et al.*, 2002; Rasmussen *et al.*, 2016; Waelbroeck *et al.*, 2019). Heinrich Events H2 and H1 are highlighted (Bond *et al.*, 1992). (C) $\delta^{18}O$ concentrations, Greenland Stadials (GS) and Interstadials (GI) from the GISP2 and GRIP Greenland ice cores (Rasmussen *et al.*, 2014), and modelled surface air temperatures relative to the present for land masses north of ~45°N (Bintanja *et al.*, 2005). (D) Sea surface temperature (SST) records determined for the North Atlantic using SST (°C) calculated using planktonic foraminifera for core SO82-02 at 59°N, 31°W (red line) (Van Kreveld *et al.*, 2000; Rasmussen *et al.*, 2016) plotted using an updated age model (Waelbroeck *et al.*, 2019) and the MD01-2461 site from the Porcupine Seabight at 51.7°N, 12.9°W (blue line) (Peck *et al.*, 2006, 2007). (E) Ice volume equivalent sea level (Lambeck *et al.*, 2014) and water depths in the central Slyne Trough using modelled relative sea levels derived from an updated glacial isostatic adjustment model (S. Bradley, unpublished data). (F) Mean and quartile ice front bed elevations estimated from the EMODnet bathymetry (www.emodnethydrography.eu/) datasets fitted against the modelled ice retreat ages. [Color figure can be viewed at wileyonlinelibrary.com]

control of a pre-existing glacigenic depocentre, and the normal bed slope of the seafloor. A positive feedback may have ensued in which sediment delivery to the grounding-line resulted in a shoaling effect acting to reduce water depths at the grounding line promoting further stabilization (cf. Alley *et al.*, 2007).

Ice-sheet retreat across Porcupine Bank to the Mid-Shelf Grounding Zone Complex (Boundary Layers 1 and 5, respectively, Fig. 12) occurred at a net average rate of ~19 m a^{-1}. However, this estimate does not consider the evidence for oscillations or readvances during deglaciation of the bank. If we estimate the retreat rate from the readvance position at ~25 ka BP (Boundary Layer 3) back to the Mid-Shelf Grounding Zone Complex (Boundary Layer 5) the retreat rate increases to ~30 m a^{-1}. The ice sheet was oscillating at the Mid-Shelf Grounding Zone Complex by 23.7 ka BP, and had receded to the Aran Islands by 22.0 ka BP where it apparently underwent a stillstand until at least 19.5 ka BP. This implies a retreat rate across the mid-shelf of ~62 m a^{-1}. The duration of the stillstand on Aran probably reflects the physiographic control imparted by the islands, which would have acted to stabilize the grounding-line on the inner shelf. Deglaciation of Aran was complete by ~19.5 ka BP but the ice sheet took ~2 ka to retreat back to the mainland, giving a net average retreat rate of ~8 m a^{-1}. Therefore, retreat from the Mid-Shelf Grounding Zone Complex onto mainland Ireland took place during Greenland Stadial 2.1 (22.9–14.7 ka; Rasmussen *et al.*, 2014) (Fig. 13C), again implying that atmospheric warming was unlikely to have been a significant control on retreat across the mid- and inner shelf.

Collectively, the above figures imply relatively slow, oscillatory retreat across the Porcupine Bank, even allowing for retreat along the reverse bed slope of the outer Slyne Trough, until the ice sheet grounded on the mid-shelf. The net retreat rate doubled across the normal bed slope of the mid-shelf to the Aran Islands where the ice sheet stabilized, and then underwent slow retreat back to the mainland. It is notable these rates are 1–2 orders of magnitude lower than retreat rates for present-day ice streams (e.g. 0.5–2 km a^{-1}; Park *et al.*, 2013; Rignot *et al.*, 2014; Scheuchl *et al.*, 2016). Such slow, episodic and oscillatory retreat is consistent with the geomorphological and sedimentological record of retreat across the Malin Shelf north-west of Ireland, which is characterized by numerous GZWs, moraines and overridden deglacial sediments (cf. Callard *et al.*, 2018; Ó Cofaigh *et al.*, 2012a, 2019). The overall slow retreat is inferred to reflect the control of bathymetry. Shallow water depths on the Porcupine Bank itself would have facilitated grounding-line stabilization and oscillations, as would the normal bedslope across the mid-inner shelf (cf. Peters *et al.*, 2016; Callard *et al.*, 2020). A topographic control on retreat across the mid- and inner shelf may have been augmented by climate cooling during retreat, as it occurred during Greenland Stadial 2.1 (Rasmussen *et al.*, 2014).

Conclusions

- Marine-geophysical data and radiocarbon-dated sediment cores, combined with TCN and OSL dating of onshore ice-marginal landforms, are used to reconstruct the timing and style of ice sheet retreat across the Atlantic shelf west of

Ireland and the adjoining coastline during the last deglaciation.

- Subglacial tills, moraines and GZWs record an extensive ice sheet at the LGM that terminated on the outermost Porcupine Bank, a westwards extension of the Irish continental shelf.
- Radiocarbon ages on reworked shells in the tills indicate the ice sheet was grounded on the outer shelf at ~26.8 ka BP.
- Grounding-line retreat in a glacimarine environment was underway by 25.9 ka BP. Retreat was punctuated by stillstands and oscillations/readvances, as recorded by overridden glacimarine sediments, moraines and GZWs. The grounding-line had retreated inshore of Porcupine Bank by 24.3 ka BP and stabilized on the mid-shelf by 23.7-ka BP, forming a large depocentre, the 'Mid-Shelf Grounding-Zone Complex'. Overall net retreat rates during this phase were 19–30 m a^{-1}.
- The ice sheet had receded to the Aran Islands by ~22.0 ka BP where it stabilized until ~19.5 ka BP, probably reflecting the topographic control of the islands which would have acted as pinning points. Overall net retreat rates across the mid-shelf were ~62 m a^{-1}.
- The timing of ice-margin recession from the Aran Islands onto mainland Ireland is constrained by numerous TCN ages on ice-transported boulders and glacially eroded bedrock as well as several OSL ages on deglacial outwash. These dates indicate that retreat across this marine–terrestrial transition took ~2 ka and was slow (8 m a^{-1}).
- Retreat of the BIIS on the Atlantic shelf west of Ireland early during the gLGM implies that external forcing by atmospheric warming was not the main driver of initial retreat. Rather deglaciation was probably at least partially triggered by high RSL reflecting a combination of eustatic and glacioisostatic components.
- Ice-sheet retreat across the shelf was characterized by numerous stillstands and oscillations of the grounding-line, but it is notable that overall retreat rates were slow. Slow retreat across the mid-inner shelf was probably controlled by a normal bedslope and the substantial pinning point of the Aran Islands. The findings here underline the importance of localized controls, specifically bed topography, on modulating the rate of retreat of marine-based sectors of ice sheets.

Acknowledgements. This research was funded by the UK Natural Environment Research Council grant NE/J007196/1 'Britice-Chrono'. The work was supported by the NERC Radiocarbon Facility (Allocation No. 1722.0613 and 1878.1014). Thanks are due to the staff at the SUERC AMS Laboratory, East Kilbride, for carbon isotope measurements, and to Sally Morgan and Elke Hanenkamp (University of Leicester) for acquisition and processing of the multi-sensor core-logger data. We gratefully acknowledge the Irish Marine Institute and the Geological Survey of Ireland for access to the INSS and INFOMAR multibeam datasets. We thank the officers and crew of the *RRS James Cook* for their assistance with data acquisition, as well as the British Geological Survey and UK National Oceanography Centre for vibro- and piston core collection, respectively, during cruise JC106. We are grateful to Caroline Clason and an anonymous reviewer whose helpful comments led to improvements to the manuscript.

Data availability

All relevant data will be made available in the forthcoming BRITICE-CHRONO online data repository, or upon reasonable request from the lead author.

Supporting information

Additional supporting information can be found in the online version of this article.

Figure a. Lithofacies logs of sediment cores from the Porcupine Bank showing calibrated radiocarbon dates. 'ID' refers to radiocarbon dates that were indistinguishable from background. The graph alongside the core logs presents the wet bulk density results (solid grey line) and magnetic susceptibility (black dashed line). Note the magnetic susceptibility scale changes between cores.

Figure b. Lithofacies logs of sediment cores from the Slyne Trough showing calibrated radiocarbon dates. 'ID' refers to radiocarbon dates that were indistinguishable from background. The graph alongside the core logs presents the wet bulk density results (solid grey line) and magnetic susceptibility (black dashed line). Note the magnetic susceptibility scale changes between cores.

Abbreviations. BIIS, British–Irish Ice Sheet; GS, Greenland Stadial; GZW, grounding-zone wedge; INFOMAR, Integrated Mapping for the Sustainable Development of Ireland's Marine Resource; INSS, Irish National Seabed Survey; LFA, lithofacies association; LGM, Last Glacial Maximum; MSCL, multi-sensor core logger; OSL, optically stimulated luminescence; RSL, relative sea level; TCN, terrestrial cosmogenic nuclide.

References

Alley RB, Anandakrishnan S, Dupont TK *et al.* 2007. Effect of sedimentation on ice-sheet grounding-line stability. *Science* **315**: 1838–1841.

Ballantyne CK, Stone JO. 2015. Trimlines, blockfields and the vertical extent of the last ice sheet in southern Ireland. *Boreas* **44**: 277–287.

Ballantyne CK, McCarroll D, Stone JO. 2007. The Donegal ice dome, northwest Ireland: dimensions and chronology. *Journal of Quaternary Science* **22**: 773–783.

Ballantyne CK, McCarroll D, Stone JO. 2011. Periglacial Trimlines and the extent of the Kerry–Cork Ice Cap, SW Ireland. *Quaternary Science Reviews* **30**: 3834–3845.

Ballantyne CK, Ó Cofaigh C. 2017. The last Irish Ice Sheet: extent and chronology. In *Advances in Irish Quaternary Studies*, Coxon P, McCarron S, Mitchell F, O'Connell M (eds). *Atlantis Press: Paris*; 101–149.

Ballantyne CK, Stone JO, McCarroll D. 2008. Dimensions and chronology of the last ice sheet in Western Ireland. *Quaternary Science Reviews* **27**: 185–200.

Batchelor CL, Dowdeswell JA. 2015. Ice-sheet grounding-zone wedges (GZWs) on high-latitude continental margins. *Marine Geology* **363**: 65–92.

Benetti S, Dunlop P, Ó Cofaigh CÓ. 2010. Glacial and glacially related features on the continental margin of northwest Ireland mapped from marine geophysical data. *Journal of Maps* **6**: 14–29.

Benn DI, Evans DJA. 1996. The interpretation and classification of subglacially-deformed materials. *Quaternary Science Reviews* **15**: 23–52.

Berger A, Loutre MF. 1991. Insolation values for the climate of the last 10 million years. *Quaternary Science Reviews* **10**: 297–317.

Bintanja R, van de Wal RSW, Oerlemans J. 2005. Modelled atmospheric temperatures and global sea levels over the past million years. *Nature* **437**: 125–128.

Bond G, Heinrich H, Broecker W *et al.* 1992. Evidence for massive discharges of icebergs into the North Atlantic Ocean during the last glacial period. *Nature* **360**: 245–249.

Bowen DQ, Phillips FM, McCabe AM *et al.* 2002. New data for the Last Glacial Maximum in Great Britain and Ireland. *Quaternary Science Reviews* **21**: 89–101.

Bradwell T, Stoker MS, Golledge NR *et al.* 2008. The northern sector of the last British Ice Sheet: maximum extent and demise. *Earth-Science Reviews* **88**: 207–226.

Bronk Ramsey C. 2009. Bayesian analysis of radiocarbon dates. *Radiocarbon* **51**: 337–360.

Callard SL, Ó Cofaigh C, Benetti S *et al.* 2020. Oscillating retreat of the last British–Irish Ice Sheet on the continental shelf offshore Galway Bay, western Ireland. *Marine Geology* **420**.106087

Callard SL, Ó Cofaigh CÓ, Benetti S *et al*. 2018. Extent and retreat history of the Barra Fan Ice Stream offshore western Scotland and Northern Ireland during the last glaciation. *Quaternary Science Reviews* **201**: 280–302.

Charlesworth JK. 1928. The glacial retreat from central and southern Ireland. *Quarterly Journal of the Geological Society* **84**: 293–344.

Chiverrell RC, Smedley RK, Small D *et al*. 2018. Ice margin oscillations during deglaciation of the northern Irish Sea Basin. *Journal of Quaternary Science* **33**: 739–762.

Chiverrell RC, Thomas GSP. 2010. Extent and timing of the Last Glacial Maximum (LGM) in Britain and Ireland: a review. *Journal of Quaternary Science* **25**: 535–549.

Chiverrell RC, Thrasher IM, Thomas GSP *et al*. 2013. Bayesian modelling the retreat of the Irish Sea Ice Stream. *Journal of Quaternary Science* **28**: 200–209.

Clark CD, Hughes ALC, Greenwood SL *et al*. 2012. Pattern and timing of retreat of the last British–Irish Ice Sheet. *Quaternary Science Reviews* **44**: 112–146.

Clark PU, Dyke AS, Shakun JD *et al*. 2009. The Last Glacial Maximum. *Science* **325**: 710–714.

Craven KF, McCarron S, Monteys X *et al*. 2021. Interaction of multiple ice streams on the Malin Shelf during deglaciation of the last British–Irish Ice Sheet. *Journal of Quaternary Science* **36**: 153–168.

Davies GLH, Stephens N. 1978. *The Geomorphology of the British Isles: Ireland*. Methuen: London.

Domack EW. 1984. Rhythmically bedded glaciomarine sediments on Whidey Island, Washington. *Journal of Sedimentary Petrology* **54**: 589–602.

Dorschel B, Wheeler AJ, Monteys X *et al*. 2010 *Atlas of the Deep-Water Seabed*. Dublin: Springer.

Dowdeswell JA, Fugelli EMG. 2012. The seismic architecture and geometry of grounding-zone wedges formed at the marine margins of past ice sheets. *Geological Society of America Bulletin* **124**: 1750–1761.

Dowdeswell JA, Ottesen D, Evans J *et al*. 2008. Submarine glacial landforms and rates of ice-stream collapse. *Geology* **36**: 819–822.

Dowdeswell JA, Whittington RJ, Marienfeld P. 1994. The origin of massive diamicton facies by iceberg rafting and scouring, Scoresby Sund, East Greenland. *Sedimentology* **41**: 21–35.

Dunlop P, Sacchetti F, Benetti S *et al*. 2011. Mapping Ireland's glaciated continental margin using marine geophysical data. In *Geomorphological Mapping: Methods and Applications: A Professional Handbook of Techniques and Applications (Developments in Earth Surface Processes)*, Smith MJ, Paron P, Griffiths JS (eds). Elsevier: Amsterdam; 337–355.

Dunlop P, Shannon R, McCabe M *et al*. 2010. Marine geophysical evidence for ice sheet extension and recession on the Malin Shelf: new evidence for the western limits of the British Irish Ice Sheet. *Marine Geology* **276**: 86–99.

Edwards R, Craven K. 2017. Relative sea-level change around the Irish coast. In *Advances in Irish Quaternary Studies*, Coxon P, McCarron S, Mitchell F (eds). *Atlantis Press: Amsterdam*; 181–215.

England JH, Furze MFA, Doupé JP. 2009. Revision of the NW Laurentide Ice Sheet: implications for paleoclimate, the northeast extremity of Beringia, and Arctic Ocean sedimentation. *Quaternary Science Reviews* **28**: 1573–1596.

Evans DJA. 2018. *Till: A Glacial Process Sedimentology*. Wiley=-Blackwell, Chichester.

Evans DJA, Ó Cofaigh CÓ. 2003. Depositional evidence for marginal oscillations of the Irish Sea ice stream in southeast Ireland during the last glaciation. *Boreas* **32**: 76–101.

Evans DJA, Phillips ER, Hiemstra JF *et al*. 2006. Subglacial till: formation, sedimentary characteristics and classification. *Earth-Science Reviews* **78**: 115–176.

Evans J, Pudsey CJ, Ó Cofaigh C *et al*. 2005. Late Quaternary glacial history, flow dynamics and sedimentation along the eastern margin of the Antarctic Peninsula Ice Sheet. *Quaternary Science Reviews* **24**: 741–774.

Evans J, Ó Cofaigh C, Dowdeswell JA *et al*. 2009. Marine geophysical evidence for former expansion and flow of the Greenland Ice Sheet across the north-east Greenland continental shelf. *Journal of Quaternary Science* **24**: 279–293.

Eyles CH, Eyles N. 2000. Subaqueous mass flow origin for Lower Permian diamictites and associated facies of the Grant Group, Barbwire Terrace, Canning Basin, Western Australia. *Sedimentology* **47**: 343–356.

Eyles N, McCabe AM. 1989. The Late Devensian (<22,000 BP) Irish Sea Basin: the sedimentary record of a collapsed ice sheet margin. *Quaternary Science Reviews* **8**: 307–351.

Graham AGC, Larter RD, Gohl K *et al*. 2010. Flow and retreat of the Late Quaternary Pine Island-Thwaites palaeo-ice stream, West Antarctica. *Journal of Geophysical Research* 115.

Haapaniemi AI, Scourse JD, Peck VL *et al*. 2010. Source, timing, frequency and flux of ice-rafted detritus to the northeast Atlantic margin, 30–12 ka: testing the Heinrich precursor hypothesis. *Boreas* **39**: 576–591.

Hallissy T. 1914. Clare Island Survey, Part 7. Geology. *Proceedings of the Royal Irish Academy. Section B* **31**: 1–22.

Hambrey MJ, Davies JR, Glasser NF *et al*. 2001. Devensian glacigenic sedimentation and landscape evolution in the Cardigan area of southwest Wales. *Journal of Quaternary Science* **16**: 455–482.

Hesse R, Khodabakhsh S, Klaucke I *et al*. 1997. Asymmetrical turbid surface-plume deposition near ice-outlets of the Pleistocene Laurentide Ice Sheet in the Labrador Sea. *Geo-Marine Letters* **17**: 179–187.

Hiemstra JF, Evans DJA, Scourse JD *et al*. 2006. New evidence for a grounded Irish Sea glaciation of the Isles of Scilly, UK. *Quaternary Science Reviews* **25**: 299–309.

Hogan KA, Dowdeswell JA, Ó Cofaigh C *et al*. 2012. Glacimarine sedimentary processes and depositional environments in an embayment fed by West Greenland ice streams. *Marine Geology* **311–314**: 1–16.

Hogan KA, Ó Cofaigh C, Jennings AE *et al*. 2016. Deglaciation of a major palaeo-ice stream in Disko Trough, west Greenland. *Quaternary Science Reviews* **147**: 5–26.

Howe JA, Stoker MS, Woolfe KJ. 2001. Deep-marine seabed erosion and gravel lags in the northwestern Rockall Trough, North Atlantic Ocean. *Journal of the Geological Society* **158**: 427–438.

Kilfeather AA, Ó Cofaigh C, Lloyd JM, *et al*. 2011. Ice stream retreat and ice shelf history in Marguerite Bay, Antarctic Peninsula: sedimentological and foraminiferal signatures. *Geological Society of America Bulletin* **123**: 997–1015.

King EL, Haflidason H, Sejrup HP *et al*. 1998. End Moraines on the Northwest Irish Continental Shelf.Third ENAM II Rorkshop, Edinburgh (abstract volume).

Knight J, Coxon P, McCabe AM *et al*. 2004. Pleistocene glaciations in Ireland. In, Ehlers J, Gibbard PL, eds. *Quaternary glaciations - extent and chronology*. Elsevier: Rotterdam; 183–191.

Lambeck K, Rouby H, Purcell A *et al*. 2014. Sea level and global ice volumes from the Last Glacial Maximum to the Holocene. *Proceedings of the National Academy of Sciences of the United States of America* **111**: 15296–15303.

Longva O, Bakkejord KJ. 1990. Iceberg deformation and erosion in soft sediments, southeast Norway. *Marine Geology* **92**: 87–104.

Lucchi RG, Camerlenghi A, Rebesco M *et al*. 2013. Postglacial sedimentary processes on the Storfjorden and Kveithola trough mouth fans: significance of extreme glacimarine sedimentation. *Global and Planetary Change* **111**: 309–326.

Mackiewicz NE, Powell RD, Carlson PR *et al*. 1984. Interlaminated ice-proximal glacimarine sediments in Muir Inlet, Alaska. *Marine Geology* **57**: 113–147.

McCabe AM, Clark PU, Clark J. 2007. Radiocarbon constraints on the history of the western Irish ice sheet prior to the Last Glacial Maximum. *Geology* **35**: 147–150.

McCarron S, Praeg D, Ó Cofaigh C *et al*. 2018. A Plio-Pleistocene sediment wedge on the continental shelf west of central Ireland: the Connemara Fan. *Marine Geology* **399**: 97–114.

Moros M, Kuijpers A, Snowball I *et al*. 2002. Were glacial iceberg surges in the North Atlantic triggered by climatic warming? *Marine Geology* **192**: 393–417.

Mulder T, Alexander J. 2001. The physical character of subaqueous sedimentary density flows and their deposits. *Sedimentology* **48**: 269–299.

Naylor D, Shannon P, Murphy N. 1999. *Irish Rockall Basin Region – A Standard Structural Nomenclature System*. Petroleum Affairs Division, Special Publication 1/99: Dublin.

Naylor D, Shannon PM. 2009. Geology of offshore Ireland. In *Geology of Ireland*. 2nd edn, Holland CH, Sanders IS (eds). Dunedin Academic Press: Edinburgh; 405–460.

Ó Cofaigh C, Dowdeswell J. 2001. Laminated sediments in glacimarine environments: diagnostic criteria for their interpretation. *Quaternary Science Reviews* **20**: 1411–1436.

Ó Cofaigh C, Dunlop P, Benetti S. 2012a. Marine geophysical evidence for Late Pleistocene ice sheet extent and recession on the continental shelf off north-west Ireland. *Quaternary Science Reviews* **44**: 147–159.

Ó Cofaigh C, Evans DJA. 2001. Deforming bed conditions associated with a major ice stream of the last British ice sheet. *Geology* **29**: 795–798.

Ó Cofaigh C, Evans DJA, Hiemstra JF. 2011. Formation of a stratified subglacial 'till' (glacitectonite) assemblage by ice-marginal thrusting and glacier overriding. *Boreas* **40**: 1–14.

Ó Cofaigh C, Evans J, Dowdeswell JA *et al*. 2007. Till characteristics, genesis and transport beneath Antarctic paleo-ice streams. *Journal of Geophysical Research* **112**: F03006.

Ó Cofaigh C, Larter RD, Dowdeswell JA *et al*. 2005. Flow of the West Antarctic Ice Sheet on the continental margin of the Bellingshausen Sea at the Last Glacial Maximum. *Journal of Geophysical Research: Solid Earth* **110**.

Ó Cofaigh C, Telfer MW, Bailey RM *et al*. 2012b. Late Pleistocene chronostratigraphy and ice sheet limits, southern Ireland. *Quaternary Science Reviews* **44**: 160–179.

Ó Cofaigh C, Weilbach K, Lloyd JM *et al*. 2019. Early deglaciation of the British-Irish Ice Sheet on the Atlantic shelf northwest of Ireland driven by glacioisostatic depression and high relative sea level. *Quaternary Science Reviews* **208**: 76–96.

Ó Cofaigh C, Dowdeswell JA, Jennings AE *et al*. 2013. An extensive and dynamic ice sheet on the West Greenland shelf during the last glacial cycle. *Geology* **41**: 219–222.

Ó Cofaigh C, Dowdeswell JA, Evans J *et al*. 2008. Geological constraints on Antarctic palaeo-ice-stream retreat. *Earth Surface Processes and Landforms* **33**: 513–525.

Orme AR. 1967. Drumlins and the Weichsel glaciation of Connemara. *Irish Geography* **5**: 262–274.

Ottesen D, Dowdeswell JA. 2009. An inter-ice stream glaciated margin: submarine landforms and a geomorphic model based on marine-geophysical data from Svalbard. *Geological Society of America Bulletin* **121**: 1647–1665.

Park JW, Gourmelen N, Shepherd A *et al*. 2013. Sustained retreat of the Pine Island Glacier. *Geophysical Research Letters* **40**: 2137–2142.

Peck VL, Hall IR, Zahn R *et al*. 2006. High resolution evidence for linkages between NW European ice sheet instability and Atlantic meridional overturning circulation. *Earth and Planetary Science Letters* **243**: 476–488.

Peck VL, Hall IR, Zahn R *et al*. 2007. The relationship of Heinrich events and their European precursors over the past 60 ka BP: a multi-proxy ice-rafted debris provenance study in the north east Atlantic. *Quaternary Science Reviews* **26**: 862–875.

Peters JL, Benetti S, Dunlop P *et al*. 2015. Maximum extent and dynamic behaviour of the last British–Irish Ice Sheet west of Ireland. *Quaternary Science Reviews* **128**: 48–68.

Peters JE, Benetti S, Dunlop P *et al*. 2016. Sedimentology and chronology of the advance and retreat of the last British–Irish Ice Sheet on the continental shelf west of Ireland. *Quaternary Science Reviews* **140**: 101–124.

Peters JL, Benetti S, Dunlop P *et al*. 2020. Sedimentary and foraminiferal records of Late Quaternary environmental change west of Ireland and implications for the last British–Irish Ice Sheet. *Journal of Quaternary Science* **35**: 609–624.

Postma G. 1986. Classification for sediment gravity-flow deposits based on flow conditions during sedimentation. *Geology* **14**: 291–294.

Powell RD. 2003. Subaquatic landsystems: fjords. In *Glacial Landsystems*, Evans DJA (ed.). *Arnold*: London; 313–347.

Powell RD, Domack EW. 1995. Modern glaciomarine environments. In *Glacial Environments*. **1**, Menzies J (ed.). Butterworth-Heinemann: Oxford, USA; 445–486.

Rasmussen SO, Bigler M, Blockley SP *et al*. 2014. A stratigraphic framework for abrupt climatic changes during the Last Glacial period based on three synchronized Greenland ice-core records: refining and extending the INTIMATE event stratigraphy. *Quaternary Science Reviews* **106**: 14–28.

Rasmussen TL, Thomsen E, Moros M. 2016. North Atlantic warming during Dansgaard-Oeschger events synchronous with Antarctic warming and out-of-phase with Greenland climate. *Scientific Reports* **6**: 20535.

Reimnitz E, Kempema EW. 1982. Dynamic ice-wallow relief of northern Alaska's nearshore. *Journal of Sedimentary Petrology* **52**: 451–461.

Rignot E, Mouginot J, Morlighem M *et al*. 2014. Widespread, rapid grounding line retreat of Pine Island, Thwaites, Smith, and Kohler glaciers, West Antarctica, from 1992 to 2011. *Geophysical Research Letters* **41**: 3502–3509.

Roberts DH, Evans DJA, Callard SL *et al*. 2018. Ice marginal dynamics of the last British–Irish Ice Sheet in the southern North Sea: ice limits, timing and the influence of the Dogger Bank. *Quaternary Science Reviews* **198**: 181–207.

Roberts DH, Hart JK. 2005. The deforming bed characteristics of a stratified till assemblage in northeast Anglia, UK: investigating controls on sediment rheology and strain signatures. *Quaternary Science Reviews* **24**: 123–140.

Roberts DH, Ó Cofaigh C, Ballantyne CK *et al*. 2020. The deglaciation of the western sector of the Irish Ice Sheet from the inner continental shelf to its terrestrial margin. *Boreas* **49**: 438–460.

Sacchetti F, Benetti S, Ó Cofaigh C *et al*. 2012. Geophysical evidence of deep-keeled icebergs on the Rockall Bank, northeast Atlantic Ocean. *Geomorphology* **159–160**: 63–72.

Scheuchl B, Mouginot J, Rignot E *et al*. 2016. Grounding line retreat of Pope, Smith, and Kohler Glaciers, West Antarctica, measured with Sentinel-1a radar interferometry data. *Geophysical Research Letters* **43**: 8572–8579.

Scourse JD, Haapaniemi AI, Colmenero-Hidalgo E *et al*. 2009. Growth, dynamics and deglaciation of the last British–Irish Ice Sheet: the deep-sea ice-rafted detritus record. *Quaternary Science Reviews* **28**: 3066–3084.

Scourse JD, Saher M, Van Landeghem KJJ *et al*. 2019. Advance and retreat of the marine-terminating Irish Sea Ice Stream into the Celtic Sea during the last glacial: timing and maximum extent. *Marine Geology* **412**: 53–68.

Sejrup HP, Hjelstuen BO, Torbjørn Dahlgren KIT *et al*. 2005. Pleistocene glacial history of the NW European continental margin. *Marine and Petroleum Geology* **22**: 1111–1129.

Shipp SS, Anderson JB, Domack EW. 1999. Late Pleistocene–Holocene retreat of the West Antarctic Ice-Sheet system in the Ross Sea: Part 1 – Geophysical results. *Geological Society of America Bulletin* **111**: 1486–1516.

Shipp SS, Wellner JS, Anderson JB. 2002. Retreat signature of a polar ice stream: sub-glacial geomorphic features and sediments from the Ross Sea, Antarctica. In *Glacier-Influenced Sedimentation on High-Latitude Continental MarginsGeological Society, London, Special Publication*, Dowdeswell JA, Ó Cofaigh C (eds). **203**: 277–304.

Small D, Benetti S, Dove D *et al*. 2017. Cosmogenic exposure age constraints on deglaciation and flow behaviour of a marine-based ice stream in western Scotland, 21–16 ka. *Quaternary Science Reviews* **167**: 30–46.

Small D, Smedley RK, Chiverrell RC *et al*. 2018. Trough geometry was a greater influence than climate-ocean forcing in regulating retreat of the marine-based Irish-Sea Ice Stream. *GSA Bulletin* **130**: 1981–1999.

Smedley RK, Scourse JD, Small D *et al*. 2017. New age constraints for the limit of the British–Irish Ice Sheet on the Isles of Scilly. *Journal of Quaternary Science* **32**: 48–62.

Smith JA, Graham AGC, Post AL *et al*. 2019. The marine geological imprint of Antarctic ice shelves. *Nature Communications* **10**: 5635.

Stewart TJ, Stagpoole VM, Wood RA. 2016. Ploughmarks and pits on the Chatham Rise: recod of deep-keeled Antarctic icebergs at 43°20′ S. In *Atlas of Submarine Glacial Landforms: Modern, Quaternary and Ancient*, **46**, Dowdeswell JA, Canals M, Jakobsson M, Todd BJ, Dowdeswell EK, Hogan KA (eds). Geological Society: London; 275–276.

Synge FM. 1965. The glaciation of west mayo. *Irish Geography* **5**: 372–386.

Synge FM. 1979. Quaternary glaciation in Ireland. *Quaternary Newsletter* **28**: 1–18.

Talling PJ, Masson DG, Sumner EJ *et al*. 2012. Subaqueous sediment density flows in different settings. *Marine Geology* **352**: 155–182.

Thébaudeau B, Monteys X, McCarron S *et al*. 2016. Seabed geomorphology of the Porcupine Bank, *West of Ireland*. *Journal of Maps* **12**: 947–958.

Thomas GSP, Connell RJ. 1985. Iceberg drop, dump and grounding structures from Pleistocene glaciolacustrine sediments, Scotland. *Journal of Sedimentary Petrology* **55**: 243–249.

Van Kreveld S, Sarnthein M, Erlenkeuser H *et al*. 2000. Potential links between surging ice sheets, circulation changes, and the Dansgaard-Oeschger Cycles in the Irminger Sea, 60-18 Kyr. *Paleoceanography* **15**: 425–442.

Van Landeghem KJJ, Chiverrell RC. 2020. Bed erosion during fast ice streaming regulated the retreat dynamics of the Irish Sea Ice Stream. *Quaternary Science Reviews* **245**: 106526.

Waelbroeck C, Lougheed BC, Vazquez Riveiros N *et al*. 2019. Consistently dated Atlantic sediment cores over the last 40 thousand years. *Scientific Data* **6**: 165.

Wanamaker AD, Jr, Butler PG, Scourse JD *et al*. 2012. Surface changes in the North Atlantic meridional overturning circulation during the last millennium. *Nature Communications* **3**: 899.

Warren WP. 1991. Fenitian (Midlandian) glacial deposits and glaciation in Ireland and the adjacent offshore regions. In *Glacial Deposits of Great Britain and Ireland*, Ehlers J, Gibbard PL, Rose J (eds). Balkema: Rotterdam; 79–88.

Warren WP. 1992. Drumlin orientation and the pattern of glaciation in Ireland. *Sveriges Geol Undersøkelse* **81**: 359–366.

Woodworth-Lynas CMT, Josenhans HW, Barrie JV *et al*. 1991. The physical processes of seabed disturbance during iceberg grounding and scouring. *Continental Shelf Research* **11**: 939–961.

